UNIVERSIDAD COMPLUTENSE DE MADRID

FACULTAD DE CIENCIAS FÍSICAS

Máster en Astrofísica

TRABAJO DE FIN DE MÁSTER

Tras las huellas de la evolución de estrellas AGB binarias y pPNe: estudio de variabilidad con TESS

In Search of the Traces of the Evolution of AGB Binary Stars and pPNe: A Study of Variability with TESS

Arturo Pérez Roncero

Supervisado por:

Dra. Carmen Sánchez Contreras (CAB, CSIC/INTA)

Dra. Alba Aller Egea (OAN, IGN)

Curso académico 20[24-25]

Declaración responsable sobre autoría
y uso ético de herramientras de Inteligencia Artificial (IA)

Yo,

con DNI/NIE/PASAPORTE:

declaro de manera responsable que el/la presente (seleccionar opción):

Trabajo Fin de Grado (TFG)

Trabajo Fin de Máster (TFM)

Tesis Doctoral

titulado/a

es el resultado de mi trabajo intelectual personal y creativo, y ha sido elaborado de acuerdo con los principios éticos y las normas de integridad vigentes en la comunidad académica y, más específicamente, en la Universidad Complutense de Madrid.

Soy, pues, la persona autora del material aquí incluido y, cuando no ha sido así y he tomado el material de otra fuente, lo he citado o bien he declarado su procedencia de forma clara —incluidas, en su caso, herramientas de inteligencia artificial—. Las ideas y aportaciones principales incluidas en este trabajo, y que acreditan la adquisición de competencias, son mías y no proceden de otras fuentes o han sido reescritas usando material de otras fuentes.

Asimismo, aseguro que los datos y recursos utilizados son legítimos, verificables y han sido obtenidos de fuentes confiables y autorizadas. Además, he tomado medidas para garantizar la confidencialidad y privacidad de los datos utilizados, evitando cualquier tipo de sesgo o discriminación injusta en el tratamiento de la información.

En Madrid, a

FIRMA

Resumen:

El objetivo de este trabajo es caracterizar la variabilidad de estrellas evolucionadas (es decir, AGB, x-AGB, post-AGB y enanas blancas). Concretamente, este trabajo analiza la posibilidad de utilizar curvas de luz de TESS para detectar ruido rojo estocástico de alta frecuencia (flickering) en dichas estrellas. Dado que se piensa que el flickering es un indicador de binaridad, su detección en este tipo de estrellas podría permitir a estudios de seguimiento detectar estrellas simbióticas (sistemas binarios compuestos por una estrella AGB y una estrella compacta). Esto podría ayudar a entender mejor la transición entre las estrellas AGB y post-AGB, que se sospecha está influenciada por interacciones binarias, basándose en las morfologías de las nebulosas proto-planetarias alrededor de estrellas post-AGB, inexplicables de otra forma.

Seguimos de cerca los pasos de Merc, J. et al. (2024) para detectar flickering utilizando datos de TESS. Sus resultados no pudieron replicarse exactamente (particularmente la clara separación entre estrellas con flickering y estrellas aisladas). Propusimos una lista de candidatos a flickering basada en valores de RMS. Ampliamos su trabajo introduciendo dos nuevos métodos: los modelos bilineal libre y no lineal. Los métodos aplicados permitieron diferenciar los parámetros de ajuste entre los distintos tipos estelares. El parámetro no lineal γ mostró una separación particularmente clara: las fuentes con flickering se concentraron en valores bajos ($\gamma < 2.0$), mientras que las AGB aisladas y post-AGB presentaron valores consistentemente más altos. Además, los objetos del Catálogo de Variabilidad (Fetherolf et al. (2023)) y los sistemas WD+IR (Farihi et al. (2025)) también exhibieron un patrón distinto, con valores de γ más elevados y τ más reducidos respecto a las AGB aisladas.

En este trabajo también desarrollamos técnicas para la selección de una muestra de control de estrellas AGB aisladas, utilizando mediciones de Galex, TESS y Gaia. Empleamos herramientas del VO (Aladdin, TopCat, etc.) así como bibliotecas de Python (LightKurve, tpfplotter, etc.). También realizamos un estudio preliminar de variabilidad periódica. En última instancia, este trabajo ha demostrado tanto el potencial como las limitaciones de utilizar datos de TESS para la detección de flickering. La alta calidad, cadencia corta y amplia cobertura de TESS lo hacen adecuado para este tipo de investigación. Sin embargo, el tamaño de píxel grande y la banda espectral más roja limitan la precisión con la que finalmente podrían realizarse las detecciones de flickering.

Abstract:

The goal of this work is to characterize the variability of late-evolution stars (i.e. AGB, x-AGB, post-AGB and WD stars). More specifically, this work analyzes the possibility of using TESS light curves for detecting high frequency stochastic red noise (flickering) in such stars. Since flickering is thought to be a tracer for binarity, its detection could allow follow-up studies to detect symbiotic stars (binary systems composed of an AGB and a compact star). This could help us better understand the transition between AGB and post-AGB stars, which is suspected to be influenced by binary interactions, based on the otherwise unexplainable morphologies of pre-planetary nebula around post-AGB stars.

We closely followed the steps of Merc, J. et al. (2024) for detecting flickering using TESS data. Their results could not be exactly replicated (particularly the clear separation between flickering and isolated stars). We proposed a list of flickering candidates based on RMS values. We expanded upon their work by introducing 2 new methods: the free bilinear and non-linear models. We found that some separation between stellar catalogs was achieved with the non-linear fitting parameter γ: flickering sources clustered at lower values ($\gamma < 2.0$), while isolated AGB stars and post-AGB objects exhibited systematically higher values. Some general characterization was also found for objects from the Variability Catalog of Stars (Fetherolf et al. (2023)) and WD+IR (Farihi et al. (2025)) catalogs, with systematically higher γ and lower τ values than isolated AGB stars.

In this work we also developed techniques for the selection of a control sample of isolated AGB stars, using measurements from Galex, TESS and Gaia. We employed VO tools (Aladdin, TopCat, etc...) as well as Python libraries (LightKurve, tpfplotter, etc...). We also carried out a preliminary periodic variability study. Ultimately, this work has shown both the potential and limitations of using TESS data for flickering detection. The high quality, short cadence, high area coverage of TESS makes it suitable for this kind of research. However, the coarse pixel size and the redder passband limit the precision with which flickering detections might ultimately be made.

Contents

1 Introduction

1.1 Low-to-intermediate mass evolved stars: AGB and beyond

The asymptotic giant branch (AGB) is a late evolutionary phase of $1 - 8M_\odot$ stars that follows the depletion of helium inside their core. The lack of fuel at the cores forces the stars to contract, increasing its temperature until hydrogen burning can start in shells around the core. This is known as the early asymptotic giant branch (E-AGB). The contraction continues, increasing the shell fusion rate. This expands the outer layers, cooling the surface temperature, all the while increasing the star's brightness. This can be traced in color magnitude diagrams (CMD) as a steep ascend to brighter and redder regions of the diagram. Once the shells are hot enough, helium shell burning will begin too, giving way to the thermally pulsing asymptotic giant branch (TP-AGB). The hydrogen and helium shells interact with one another, periodically becoming unstable, and resulting in "thermal pulses", thousand-year long readjustments in the shells after runaway burning.

In simpler terms, AGB stars are objects with initial masses between $1 - 8M_\odot$ approaching the end of the stellar life cycle. They have highly metallic compositions, even at the surface, due to dredge-ups. Their outer shells are extremely expanded, resulting in cool effective temperatures. They are very bright ($10^3 - 10^4 \ L_\odot$) and very big ($100 - 1000 \ R_\odot$). On account of them being so large, AGB stars are susceptible to all kinds of variability mechanisms, specially pulsations or other asteroseismic phenomena.

The low gravitational pull on the outer envelopes makes AGB stars prone to mass loss, which in some cases amounts to quantities of gas large enough to create extended structures around the star. Once mass loss grinds to a halt, as a result of most of the weakly-bound outer layers already being shed, the star contracts and heats up, giving way to the so-called post-AGB phase. The post-AGB phase is characterized by usually being contained inside a pPN: gas structures originating from the star's shed layers, and theorized to be the precursors of planetary nebulae. This topic will be expanded upon in the next subsection.

1.2 Impact of, and signs of, binarity in evolved stars

As mentioned in the previous section, AGB stars have such immense radii that the gravitational pull on its outer layers becomes very weak. This facilitates mass loss to a point where large amounts of the mass of the star are being shed (from 10^{-8} to $10^{-5} \ M_\odot$ per year, amounting to a significant fraction of the star's mass being lost (Kippenhahn et al. (2012))), generating large gas structures around it, forming a pre-planetary nebula (pPN).

pPN have, more often than not, complex morphologies. It is theorized that this might be due to binary interactions, which sculpt the gas from the pPN into bipolar, multipolar, or highly axisymmetric structures. Recent surveys suggest that up to 60% of AGB stars could have main sequence companions (Ortiz and Guerrero (2016)), but confirming binarity before the star's transition to the post-AGB phase can be difficult.

Symbiotic stars are binary systems composed of a cool, evolved AGB star and a compact partner (typically a white dwarf, although rarer systems with neutron stars have also been observed (Chakrabarty and Roche (1997))). Symbiotic stars typically have wide orbits, meaning they do not exchange mass directly through Roche-lobe overflow, but strong stellar winds can nonetheless form accretion disks around the compact partner, likely producing some UV excess. This might be achieved through Wind Roche Lobe Overflow (WRLOF) (Sun et al. (2024)), where stellar winds reach the Roche Lobe, even if the extended atmosphere does not.

Accretion disks can generate recognizable signals, allowing us to infer the presence of binary companions around AGB stars before a pPN has been formed. More specifically, signals from accretion disks usually present high frequency stochastic variability (typically called flickering in the literature). As material falls onto the compact star, it gathers around a tight disk. The closer to the star, the faster it orbits. Infalling particles within the disk then interact with each other, either through viscosity or through magnetism, heating up, and emitting as a black body. However, the increase in temperature is not homogeneous, giving way to a range of regions with different sizes emitting at different temperatures. These regions evolve rapidly, changing in both size and temperature, and causing the signal to "flicker" in brightness and frequency. In other words, a fourier transform of the high frequency variability of a flickering source would reveal a high-RMS, noisy, fast-evolving spectrum that fuses itself at the highest frequencies with the intrinsic white noise of the detector.

Several space missions (such as the Hubble Space Telescope (HST) or Galex), and numerous ground-based telescopes (such as the Rozhen observatory), have observed flickering stars. This is typically done in blue or UV bands, where flickering is much brighter relative to its host star than in redder bands. UV excess particularly has gained some attention as a potential tracer for binarity (Sahai et al. (2011)), likely arising from accretion-driven interactions between the AGB wind and a companion. Similarly, X-ray detections in AGB stars (x-AGB) signal accretion too, offering additional candidates.

Some notable works researching flickering include Bruch (1992) (establishing the ground work for later studies on the flickering of cataclysmic variables), Zamanov et al. (2010) (which used data from the Rozhen observatory to characterize the flickering in RS Ophiuchi, a known symbiotic star), and Sahai et al. (2018) (which used data from HST to study flickering in UV bands in AGB stars).

Although rare, given the less favorable conditions for flickering observation, research on flickering detection using measurements in redder bands has also been done recently. Notably, Merc, J. et al. (2024) used light curves from the TESS Mission (with a 6000 - 10000 nm band pass) to first test whether flickering could be detected in symbiotic stars already known to exhibit it, and subsequently identify previously unrecognized flickering symbiotic stars. Their work will be used as reference for this work's efforts at characterizing flickering using TESS data.

For some rare cases, the ecliptic plane of the binary system coincides with our line of sight, allowing us to directly detect binaries through transits (a periodic dimming in the brightness of the star). If the binaries orbit each other at close enough distances, we can also observe the elliptic deformations of their envelopes (resulting in periodic brightness variability). Although rare, such objects can be confirmed as binaries much more easily than through flickering detection.

1.3 The TESS Mission

The Transiting Exoplanet Survey Satellite (TESS)[1] is a NASA mission launched on April 2018, and still functioning today. Its primary mission is to detect exoplanets through transits in light curves using precise photometric measurements in the T passband (6000 - 10000 nm). Despite having a much coarser spatial resolution than its predecessor, Kepler (21 vs. 4 arcseconds, respectively), TESS improves on a lot of mission critical parameters, such as: much better cadence (up to 20 second cadence light curves), much larger sky coverage (around 85% of the entire sky), and more modern CCDs that allow for much higher quality data. Plus, TESS, unlike Kepler, focuses on brighter stars closer to us, which allows higher magnitude objects, such as AGB stars, to be observed without saturating the detectors. However, the big pixel size makes it a necessity to analyze possible contaminants in crowded fields.

TESS is capable of covering such a large area of the sky because of its 4 wide angle cameras, arranged vertically from the polar region to the equator of the sky, each observing 24×24 degrees of the celestial sphere. TESS measures each region of the sky for 27 days, and assigns to the area covered by each camera a chronological sector number. Polar regions will thus be covered much more regularly, allowing certain objects to have a bonanza of measurements, but leaving equatorial objects less observed. Every year, TESS completes an entire hemisphere, and moves on to the other one. The pattern repeats indefinitely, reassigning sector numbers to previously observed sectors, differentiating them from past observations.

In order to observe both hemispheres, and to avoid contamination, TESS was put on a highly eccentric orbit around Earth. Every 13.7 days, twice per sector, and near the perigee, TESS interrupts observations in order to upload data to Earth (denominated downlink gap).

Although TESS's main mission is to detect exoplanets, one of its secondary missions is to study variable stars. A high quality, precise, 2-minute cadence light curve allows for an extensive asteroseismic analysis of stars with any kind of variability in its brightness, such as AGB stars.

However, raw data from TESS can be messy and full of outlier data points. TESS takes full-frame images (FFI) of the entire sector. But, in order to minimize downlink time, TESS does not upload to Earth all of the light curves it measures, uploading instead longer cadence FFI. The cadence of FFI have changed throughout the years, starting at 1800 seconds. As of 2025, TESS is measuring FFI with a 120 second cadence.

It is then necessary to carefully select the appropriate pixels inside the FFI that contain data from the desired object, generating an "aperture", from which photometric data can be obtained, so that a light curve for the object can be computed. The aperture can change from sector to sector for a given object. However, for a given set of TESS Objects of Interest (TOIs), TESS has already saved from the full set of FFI (prior to downlink simplification) light curves with the optimal cadence (up to 20 seconds).

Selecting the adequate data processing pipeline is crucial. Luckily, several pipelines are available on the Mikulski Archive for Space Telescopes (MAST). MIT's Quick-Look Pipeline (QLP)[2] offers light curves for most stars, but are usually noisy and have longer cadences. On the other hand, the TESS Science Processing Operations Center (SPOC)[3] offers more precise, clean light curves for TOIs. SPOC corrects the raw data from orbital and instrumental contamination, as well as from threshold crossing events (outliers). A full set of corrected FFI, cleaned through the same pipeline as SPOC lightcurves, can be found under the author name "TESS-SPOC". The latter, being FFI, will typically have longer cadences than SPOC light curves, but can be useful nonetheless.

1.4 Goals of this work

As mentioned before, the novelty of TESS is that it offers high quality, short cadence light curves for brighter stars. That means that previously uncharacterized AGB stars can now be studied much more thoroughly, and given more precise classifications according to their variability. For example, its short cadence makes TESS specially suitable for detecting flickering, high frequency stochastic variability that would otherwise be invisible in longer cadence data.

---

[1] https://exoplanets.nasa.gov/tess/
[2] https://tess.mit.edu/qlp/
[3] https://heasarc.gsfc.nasa.gov/docs/tess/data-handling.html

Thus, the goal of this work is to analyze TESS measurements of stars in advanced stages of evolution, in search of both stochastic and periodic variability. Particularly, we studied AGB, x-AGB, post-AGB, symbiotic and WD stars. The work by Merc, J. et al. (2024) will be used as reference for the detection of flickering via TESS light curves. The validation of their results will be one of the primary goals. If possible, we look to isolate the effects of binarity in the periodograms, and determine if flickering detection using TESS data is a viable tracer of binarity in evolved stars, and thus of symbiotic stars.

2 Observations and Data Processing

In this work we have analyzed TESS light curves from stars in several catalogs. These include a control sample of AGB stars from Suh (2021), the symbiotic and red giant stars studied in Merc, J. et al. (2024), post-AGB stars from Oomen et al. (2018) and Fetherolf et al. (2023), and white dwarfs with infrared excess (WD+IR) from Farihi et al. (2025). Information about these catalogs, and the motivation behind their selection, will be expanded upon in Section 2.3.3.

Table 1 gathers some over-all information about the stars selected from these catalogs. Our work analyzes a sum of 278 stars. Most stars have been observed in more than one sector, resulting in a total amount of light curves analyzed of 842. This results in large and numerous tables and graphs. In this work we will present subsets of such tables, shown for illustration, and examples of graphs. If you wish to access any specific table or graph, please refer to this GitHub page.

In Sections 2.1 and 2.2 we will first discuss the workflow employed for the data gathering, processing and analysis. This workflow includes an extensive use of Python (with libraries specific to TESS data processing), as well as tools from the Virtual Observatory (Aladdin and TopCat most notably). In Section 2.3 we will expand upon the selection process for the stars used in this work.

Table 1: Summary of Stars and Sectors by catalog.

Stellar Category	No. of objects	No. of light curves	Reference
Isolated AGB stars	155	431	Suh (2021)
Merc et. al. stars (no flickering detected)	41	113	Merc, J. et al. (2024)
Merc et. al. stars (flickering detected)	17	35	Merc, J. et al. (2024)
post-AGBs from the TESS VSC	22	105	Fetherolf et al. (2023)
post-AGB binaries (van Winkle objects)	17	31	Oomen et al. (2018)
x-AGB	13	34	Guerrero et al. (2024)
WD+IR	13	93	Farihi et al. (2025)

2.1 Using TESS data with Python: LightKurve and tpfplotter

In this work, the bulk of the data processing and analysis has been made using Python. The light curves were acquired from MAST mainly through the Python library LightKurve (Lightkurve Collaboration et al. (2018)), which allowed for filters in the data search. SPOC light curves (short cadence light curves of TESS Objects of Interest) and TESS-SPOC FFI (Full Frame Images that have been processed with the same pipeline as SPOC light curves) were downloaded for our collection of objects for every possible sector and cadence. LightKurve itself is also able to filter out from the light curves bad data identified by SPOC, as well as eliminating outliers through a 3 σ clipping, standard in the literature for the type of studies carried out in this work.

We also used the Python library tpfplotter (Aller et al. (2020)) for overlaying Gaia data onto the TESS image and identifying probable contaminants. Tpfplotter allows for the option to output the list of objects inside the TESS aperture of the light curve, making it easy to spot sources of brightness or variability that do not belong to the object of study.

2.2 Initial Data Reduction Pipeline

Once TESS light curves have been downloaded through LightKurve for the desired sectors and TIC ids (TESS Input Catalog, numeric identifier given to each star by TESS), an initial filtering out of bad data is made. First of all, due to the technical capabilities of TESS, we found that objects with a brightness greater to magnitude 4 appeared to be too saturated for the data to be reliable, and were eliminated from the sample (a total of 27 objects, 26 of them isolated AGB stars). Secondly, due to the large size of TESS's pixels, stars in crowded regions would usually have apertures containing neighboring stars. Data from these stars could sometimes be salvageable on account of near stars being faint enough, but in most cases they had to be eliminated from the sample. This "crowdedness" parameter (the amount of signal originating from the observed source, and not neighbors) was already included

in the header of the light curves as the value "CROWDSAP". A limit of CROWDSAP> 0.95 was selected as the threshold for sampled stars.

The processed light curves from TESS, once imported into Python, require some further readjustments. The PDCSAP flux column is used by default, as it has already been corrected for major instrumental effects by the TESS pipeline, unlike the raw sap_flux data. We then eliminate data points with a quality mask value other than 0. Data points that are detected as faulty by the computer onboard TESS at the time of measurement are automatically flagged by setting its quality mask to values other than 0. The exact quality mask value depends on the exact error suspected for the data point. Before further processing, the light curves were renormalized from Analog-to-Digital Unit (ADU) to Parts per million (PPM).

Once cleaned, light curves were smoothed using a Savitzky–Golay filter (Savitzky and Golay (1964)). The goal was to extract from the signal any low frequency tendency, originating from instrumental error tails around downlinks, or from intrinsic variability from the star. These low frequency tendencies were then subtracted from the light curve, isolating the high frequency fluctuations from the star. This last signal was then used to properly calculate the RMS value, further discussed in Section 3.2.

Two types of periodograms were computed for the unsmoothed light curves (without any Savitzky–Golay filter applied). This was done via the Lomb-Scargle periodogram library included in Astropy[4]. Periodograms are discrete Fourier transforms of light curves, typically made using data with uneven time steps. They calculate the presence, if any, of possible periodic variabilities in a given frequency range. A higher power value means that that given frequency is more present in the signal. As we prove in later sections, gaps of data (downlinks or holes in the light curve made from deprecating data points because of bad quality) can create artificial peaks in power in the periodogram.

First, a periodogram was made of the entire frequency spectrum. This ranges from the Nyquist frequency (the highest possible frequency inferred from the data, assuming wavelengths sampled by at least two points) to the lowest possible frequency (around 27 days, the total amount of time observed by sector). This type of periodogram is usually portrayed as a log-log plot in order to ease readability (see Figure 1c).

Secondly, a periodogram was made of the low frequency regime using a smoother, slower computational Lomb-Scargle method ("cython"). This was done with the intention of better characterizing low frequency periodic variability. In these periodograms we also calculated the False Alarm Probability values (FAP) using the Astropy Python library. These values are shown in plots (as in Figure 1e) as black horizontal lines, corresponding to a 90%, 95% and 99% chance of that peak being a false alarm. In other words, peaks in the periodogram exceeding these lines are not likely to be a result of noise, but real variability in the signal.

Once this initial data processing was finished for all objects, one last filter was carried out. Light curves were classified via visual inspection of the periodogram. As mentioned before, if the final light curve is missing too many data points in a periodic pattern (every 13 days, in the case of downlink), artificial peaks might show up in the periodogram (as the ones in Figure 1e). However, if the final light curve is missing too many data points in a non-periodic pattern, the resulting periodogram can end up incredibly distorted, usually in the shape of wide arches at high frequencies (as in Figure 1d). No further analysis can be carried out in this cases. Visual inspection also revealed probable binarity candidates, which might have strong peaks at medium frequencies (as in Figure 1c).

The initial data reduction pipeline can thus be summarized into the following steps:

1. **Data Acquisition and Filtering**
   - Download TESS light curves (LightKurve) for target stars
   - Remove saturated stars ($T_{\mathrm{mag}} < 4$)
   - Exclude crowded targets (CROWDSAP ≤ 0.95)
2. **Data Cleaning**
   - Select PDCSAP flux (instrument-corrected)
   - Remove bad-quality points (quality flag $\neq 0$)
3. **Normalization**
   - Convert flux to PPM

4. **Smoothing**
   - Apply Savitzky-Golay filter and subtract low-frequency trends for RMS calculation
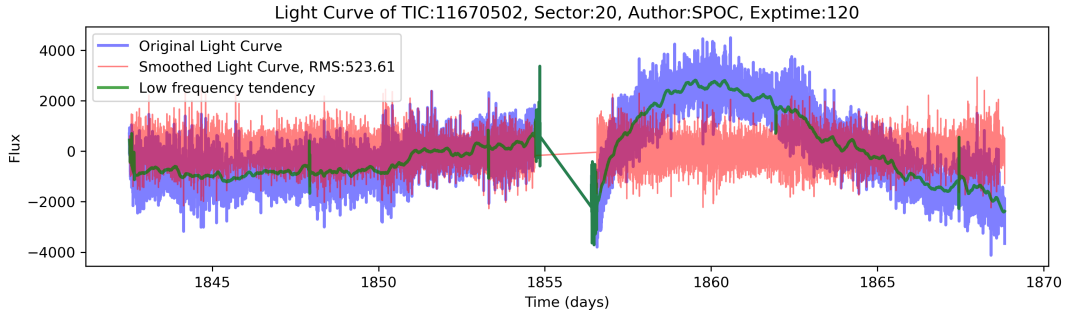5. **Periodogram Analysis**
   - Compute Lomb-Scargle periodograms (Astropy):
     - Full frequency range (log-log)
     - Low-frequency focus (linear)
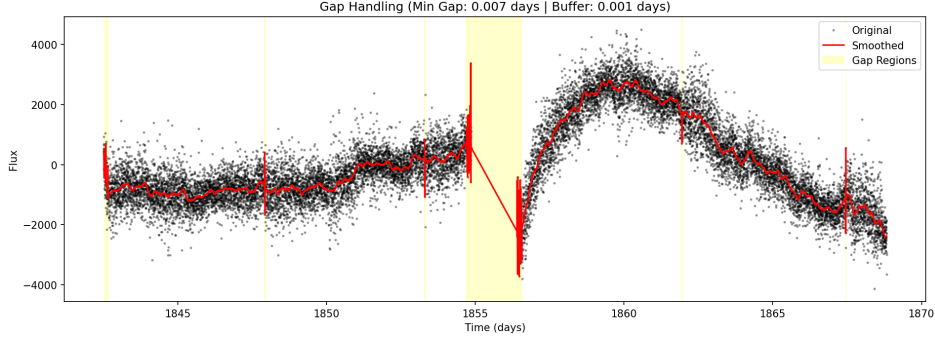   - Calculate FAP thresholds
6. **Quality Control**
   - Visually inspect for:
     - Distorted periodograms (non-periodic gaps)
     - Binary candidates (medium-frequency peaks)
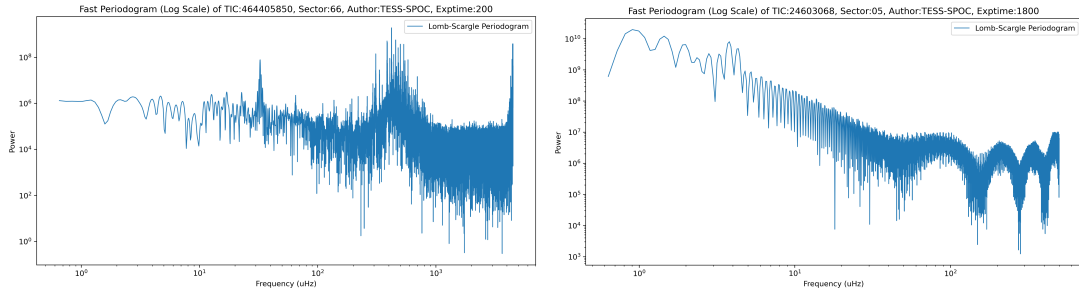   - Artificial peaks (periodic gaps)

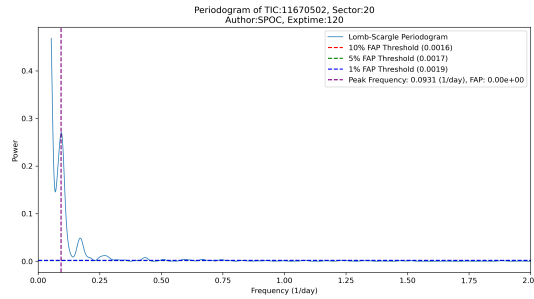[4]https://docs.astropy.org/en/stable/timeseries/lombscargle.html

(a) Raw (blue) and smoothed (green) light curves of V* SU Lyn (TIC 11670502), showing stellar variability. Raw light curve with smoothed tendencies subtracted (red). The Savitzky-Golay filter isolates low-frequency features that can later be subtracted.

(b) Troubleshooting graph showing data quality of TIC 11670502: Downlink and instrumental data gaps (regions in yellow) of the raw (black points) and smoothed (red) light curve.

(c) Example periodogram of a likely binary system. Object TIC464405850.

(d) Example periodogram of a faulty light curve. Object TIC24603068.

(e) Linear view of low-frequency peaks (< 2 d^{-1}).

Figure 1: (a-b) Light curve cleaning and smoothing; (c-d) Frequency analysis. More examples of plots can be found in Appendix, or in this GitHub page.

2.3 Samples studied in this work

2.3.1 Objects used in Merc, J. et al. (2024)

The initial goal of this work was first to validate the findings from Merc, J. et al. (2024), and then potentially improve on their method, and use it on different star samples. In order to recreate their results as faithfully as possible, we gathered all of the objects they used for their study, which can be classified into several groups: stars with no

flickering detected (Table 2, mostly AGB stars, but also symbiotic stars with no detectable flickering), objects with flickering detected via TESS light curve analysis (Table 3, which includes well-known symbiotic stars as well as previously unidentified flickering AGB stars) and a control sample of (assumed) isolated AGB stars. However, no information was given in Merc, J. et al. (2024) about the specific stars used as a control sample of isolated AGB stars. In Section 2.3.2 we explain how we selected our own sample.

Table 2: Subset of stellar parameters for AGB and and symbiotic stars in Merc, J. et al. (2024) without flickering detection using TESS light curves. The full table is available at GitHub.

Name	TIC ID	TESS mag	Sectors	CROWDSAP
BX Mon	64333488	8.61	7	0.973
EG And	115780639	5.30	17,57,84	1.000
RS Oph	6348255	9.46	80	0.959
SULyn	11670502	5.00	20,60,73	1.000
V1044 Cen	30541762	8.69	37,64	0.898
V407 Cyg	357457104	9.52	15,16,55,56,75,76,82,83	0.911
ZZCMi	453173127	6.38	87	0.999
omi Cet Mira	332890609	2.26	31,4	0.904
AE Ara	30667659	9.93	66	0.924
...				

Table 3: Subset of stellar parameters for AGB and and symbiotic stars in Merc, J. et al. (2024) with flickering detection using TESS light curves.

Name	TIC ID	TESS mag	Sectors	CROWDSAP
694 Mon	403675153	8.65	87	0.985
ASAS J152058-4519.7	146068950	9.16	65	0.929
CN Cha	394916057	7.02	64,66	0.992
RTCru	180045004	8.88	64,65	0.758
TCrB	462607643	7.73	24,25,51,78	1.000
420 Hya	443619246	7.37	37,64	1.000
AR Pav	304202168	9.82	66	0.956
AX Per	453231036	8.74	58	0.980
Hen 3-461	303495210	8.19	36,37,63	0.975
...				

2.3.2 Isolated AGB stars

As mentioned in Section 2.3.1, Merc, J. et al. (2024) does not specify the source, nor the stellar parameters for the presumably isolated red giants used as a control sample. Thus, we gathered ourselves a sample of likely isolated AGB stars, in order to characterize the effects of binarity in the periodograms, and determine if flickering detection using TESS data is a viable tracer of binarity in evolved stars. Merc, J. et al. (2024) do not specify how they chose their control sample either, so alternative methods were used in this work to find likely isolated stars. It is important to point out that it is usually extremely complicated to firmly conclude that a star is indeed isolated, given the observational biases of the different detection techniques. In symbiotic stars specifically, the brightness contrast between an AGB star and a white dwarf is so great that resolution of both stars is even more complex. We are left with indirect indicators of binarity, such as radial velocity or transits. However, these are not good for confirming isolation, since they only confirm binarity. We therefore select a sample of AGB stars statistically likely to be isolated, while recognizing that some binary systems may have been included due to the limitations of our methodology. In fact, if recent studies are to be believed, binarity might be the norm for AGB stars, instead of the exception (Ortiz and Guerrero (2016)), making our selection process even more prone to error.

In order to discard binaries from our sample, we based ourselves in the method described in Sahai et al. (2011). They found that a detection of UV light could be tied with binarity in AGB stars. This UV excess could originate from a hot, compact partner (e.g. white dwarf), or from the interaction of a possible partner with an accretion disk. Thus, eliminating from the sample AGB stars with UV excess could be a good start for reducing the amount of binaries in the sample.

We first gathered all the AGB stars included in the catalog from Suh (2021). These were cross-identified from IRAS, AKARI, MSX, WISE, 2MASS, and AAVSO catalogs; and offer a large pool from where to select likely

candidates. We then cross-matched those stars with measurements from Galex[5] (a UV space telescope launched in 2003) in both its near UV (Galex-NUV) and far UV (Galex-FUV) filters. For this we used Aladdin[6]. We also cross-matched the resulting catalog with measurments from Gaia[7] (a space telescope launched in 2014 offering precise astrometric data for a wide selection of stars), in order to correct stars of extinction and reddening, and convert apparent magnitudes to absolute magnitudes.

Before making the final sample selection, we cross-matched all stars with the the TESS catalog using TopCat[8], in order to obtain all of the star's TIC ids and TESS magnitudes. We then filtered out stars with faulty data (e.g. bad Gaia parallax results) and TESS band brightness higher than magnitude 4 (since we know we will not be able to use its TESS light curves). We also deprecated stars that were known binaries (using SIMBAD[9] queries, which offer the star's "MainType", which can help identify known spectroscopic binaries, astrometric binaries, etc...).

357 AGB stars were initially obtained from Suh (2021), from which 155 were finally selected, 10 of those being confirmed binaries in SIMBAD. Once the initial sample of AGB stars with measurements of TESS, Gaia and Galex had been arranged, we proceeded with the final sample selection, basing ourselves on the identification criteria used in Ortiz and Guerrero (2016). They claim that any star with non-zero brightness in the Galex-FUV band is likely to be a binary. They also claim, although less definitively, that AGB stars with relatively high Galex-NUV emissions were also binary candidates.

Assuming that Galex-FUV detections are indeed a proxy for probable binarity, we are faced with the fact that most of our stars have no Galex-FUV detection (around 15% of the sampled AGB stars did). If we want to further reduce the number of stars in our sample of likely isolated stars, strictly eliminating stars with Galex-FUV detections will not be enough. Thus, we need to extrapolate the features of stars that do have Galex-FUV detections, and pick the stars that deviate the most from such criteria. First, we calculated the T-NUV color index (substracting the TESS magnitude and the Galex-NUV magnitude). When a star has a value of T-NUV close to 0 it means that it is probably a binary system with a compact companion which might be contributing to the UV signal.

As seen in Figure 2a, for stars with the same T_{mag}, those with Galex-FUV detections have higher T-NUV values than those without. This results in stars with Galex-FUV detections gathering at the lower right regions of the overall linear trend. The linear fits in Figure 2a show that there is a systemic 1.5 difference in T_{mag} (vertical axis) between both types of stars. This, of course, is most likely due to a coupling between the Galex-NUV and Galex-FUV values, which is expected. In other words, stars with Galex-FUV emissions are more likely to also have Galex-NUV emissions. Nonetheless, this trend is very useful, since we can now identify stars with anomalous UV emissions even when they do not have Galex-FUV emissions, as we had intended.

We can now determine our final control sample of AGB stars by selecting only those stars towards the top left region of Figure 2a, as shown in Figure 2c. Those objects are shown in Table 4. The "Binary Likeness" parameter, ranging from 50 to 300 (quantifying the position in the final sample, containing 300 stars), quantifies how much towards the upper left corner the star is. In Section 5 we will take a value of 150 or lower as the threshold for the selection of the control sample. This was calculated by detrending the data (subtracting the linear fit from Figure 2a). Despite the final sample containing 300 stars, only 155 of those had suitable TESS data.

Table 4: Subset of stellar parameters for the final control sample catalog of likely isolated AGB stars. 357 were initially obtained from Suh (2021), from which 155 were finally selected following the filters described in Section 2.1. The full table is available at GitHub.

TIC ID	TESS mag	Sectors	CROWDSAP	Binary Likeness
147795605	7.7	60	0.968	50
336728909	10.19	57	0.999	50
354209282	6.15	56	1.0	50
91104738	5.57	56,83	1.0	50
296974016	7.93	63	0.999	50
16880539	5.31	57,84	0.997	50
139121623	3.97	27,28,68	0.999	50
431603831	9.59	57	0.907	50
24350903	2.47	42,55,82	0.994	50
...				

(a) Apparent magnitudes

(b) Absolute magnitudes

(c) Final control sample of isolated AGB candidates.
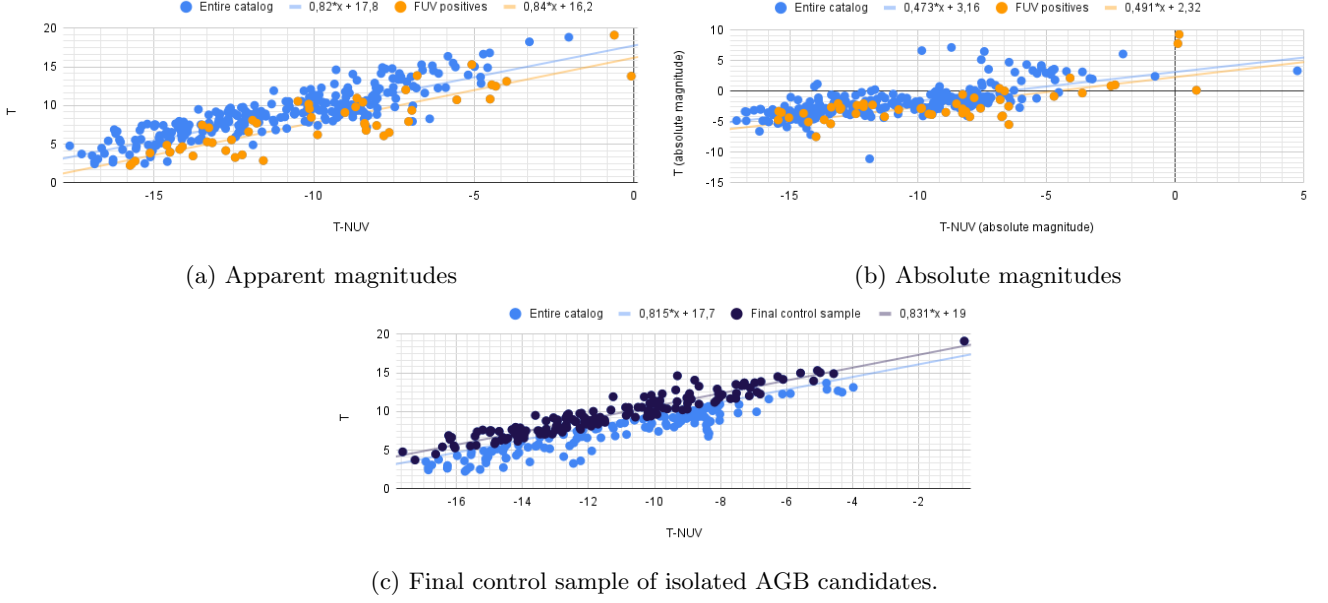
Figure 2: T vs. T-NUV for the subsample of AGB stars from Suh (2021) with TESS, Galex and Gaia measurements (light blue), stars with Galex-FUV detections (orange) and the final control sample of AGB stars (black).

2.3.3 x-AGB: AGB stars with X-ray excess

As discussed in the previous section, detection of UV in AGB stars is thought to be tied to binarity, and thus, to the presence of an accretion disk. X-ray emissions in AGB stars, although more rare, might originate from the same phenomena as UV emissions. In fact, X-ray emissions have been detected in known symbiotic stars, sometimes in a recurrent fashion that might suggest the presence of an accretion disk (Toalá et al. (2024)). These stars are thus likely candidates for flickering detection. We have selected 13 AGB stars with x-ray excess (x-AGB) from Guerrero et al. (2024) for this work (Table 5).

Table 5: Subset of stellar parameters of the 13 x-AGB stars.

Name	TIC ID	TESS mag	Sectors	CROWDSAP
CD-38_3905	132636906	8.40	61,62	0.904
HD_165774	330960059	6.06	13,66	0.989
HD_187372	272841269	4.40	14,15,41,54,55,56,74,75,82	0.999
IRAS_08427+0338	350315597	11.32	61	0.980
V*_CI_Hyi	234300677	5.26	27,29,67,69	0.998
V*_DH_Eri	178804201	5.14	31,32	1.000
V*_EY_Hya	393806122	4.69	34,61,88	0.999
V*_R_Aqr	92138849	5.36	29,69,70	1.000
V*_TW_Cen	112098802	6.43	64	0.987
...				

2.3.4 Other Objects

In addition to symbiotic stars and xAGBs (along with the control sample of presumably non-binary AGB candidates), we have also explored the variability of post-AGB stars and white dwarfs using TESS data.

As this area remains largely unexplored, to our knowledge, we investigate whether signs of flickering or other indicators of binarity can be identified, and whether different stellar populations can be distinguished based on their TESS light curve properties.

The first addition we made to our list was the catalog of post-AGB stars included in Oomen et al. (2018) (Table 6). 17 objects from this catalog were finally selected. These stars are later referred to in this work as *van Winkle* objects.

Van Winkle objects are post-AGB stars with near infrared excess, which indicates the presence of dust around the star. Further analysis of these objects revealed that they were, in fact, binaries with main sequence companions with orbital periods ranging from 1 to 10 years. They are characterized for having rotating circumbinary disks, and not particularly intense stellar winds. These characteristic made them an interesting target for our analysis of flickering.

Table 6: Subset of stellar parameters of the 17 post-AGB stars selected from Oomen et al. (2018).

Name	TIC ID	TESS mag	Sectors	CROWDSAP
89_Her	285139576	5.08	26,40,52,53,79,80	0.999
BD+46_442	327790652	8.89	58	0.978
DY_Ori	151405646	9.85	71,72	0.968
HD_108015	72069886	7.52	64	0.985
HD_131356	259921603	8.00	65	0.954
HD_213985	188569689	8.73	69	0.999
HD_46703	149984609	8.43	60	0.997
HD_52961	425148238	6.83	71,72	0.998
...				

Secondly, we included some of the objects studied in Fetherolf et al. (2023), from the so-called "Variability Catalog of Stars Observed during the TESS Prime Mission". This catalog includes a large amount of all sorts of variable objects. We only included 22 post-AGB candidate stars (stars with IRAS[10] color measurements compatible with post-AGB stars), selected based on strangely short variability periods (1 to 10 days), which made them also binary candidates. See Table 7.

Table 7: Subset of stellar parameters of the 22 used stars from the Variability Catalog of Stars Observed during the TESS Prime Mission (Fetherolf et al. (2023)). The full table is available at GitHub.

Name	TIC ID	TESS mag	Sectors	CROWDSAP
*_73_Ori	434408053	5.42	33,43,44,45,71,72,87	0.999
HD_15629	49720925	8.00	18,58	0.980
HD_161796	316493106	6.75	24,25,26	0.999
HD_239626	329074395	8.91	15,16,17,56,57,84	0.755
HD_3191	284141111	8.13	17,18,58,85	0.969
HD_36408A	302824830	6.08	43,44,45,71	0.715
HD_95862	304996702	8.74	10,11,63,64,90	0.951
LS_II_+25_15	435781776	10.60	14,41,54,81	0.911
TYC_8170-690-1	75311623	10.41	62,63	0.868
...				

Lastly, we included a set of 13 white dwarfs with excess infrared emission, a potential indicator of the presence of disks resulting from mass transfer in a binary-interacting system. We used the list included in Farihi et al. (2025) (Table 8).

Table 8: Subset of stellar parameters of 13 WD with IR excess from Farihi et al. (2025). The full table is available at GitHub.

Name	TIC ID	TESS mag	Sectors	CROWDSAP
BD+20_307	91373945	8.45	17,42,43,70,71	0.998
EC_05365-4759	220616055	15.87	31,32,33,87	0.592
GD_362	88844987	16.03	25,26,52,53,79,80	0.052
GD_85	17857475	15.07	60	0.307
HD_172555	464405850	4.62	66	0.990
PG_0843+517	142259188	16.33	20,47	0.614
SCR_J0859-3647	191233258	15.43	62,89	0.394
Ton_345	184915712	16.13	44,46,72	0.808
UCAC4_077-007106	391923441	15.28	10,11,12,13,27,28,29,30,	0.210
...				

3 Non-periodic variability: Flickering analysis in Merc, J. et al. (2024)

In this section we explore how flickering manifests in light curve analysis. Specifically, we show the theoretical shape flickering might have, how it can be correlated with the RMS, and the methodology employed for its detection in

---

[10]https://irsa.ipac.caltech.edu/Missions/iras.html

Merc, J. et al. (2024). We also explain how we tried to validate the methodology and results from Merc, J. et al. (2024). Lastly, we propose several improvements and alternative methods for flickering detection using TESS light curves.

3.1 The theory behind flickering

As discussed in Section 1.2, flickering is a stochastic, high frequency variability observed in the light curves of objects with accretion disks. The ultimate physical processes behind this phenomenon is not clear. In Uttley et al. (2005) they propose that the signal from an accretion disk can be modeled by quantifying the amount of coupling between frequencies.

White noise has no coupling, for instance. The value of a white noise has in no way been influenced by its prior values. On the other hand, coupled variability, such as that of a random walk, depends on all of its prior states (the final state of a random walk is the sum of all of its past displacements). In other words, by defining the coupling of past states with the present one, it is possible to describe variability processes that have propagation between frequency modes.

Uttley et al. (2005) find that flickering is not a white noise phenomenon, but one that shows itself in periodograms as "red noise" (where lower frequencies have more power than higher ones). Probably as a result of a coupling between smaller, faster temperature fluctuations with bigger, slower ones further away in the disk, flickering always possesses some amount of negative slope in the periodograms.

We illustrate this in Figure 3, where we plot in Figure 3a 3 different synthetic light curves (as proposed in Uttley et al. (2005)), and in Figure 3b their respective periodograms. We include white noise (no coupling between steps), a random walk (maximum coupling, resulting in a strong negative slope), and a middle ground example with some amount of coupling. Theoretical slopes for flickering in log-log plots range from -1.5 to -2.

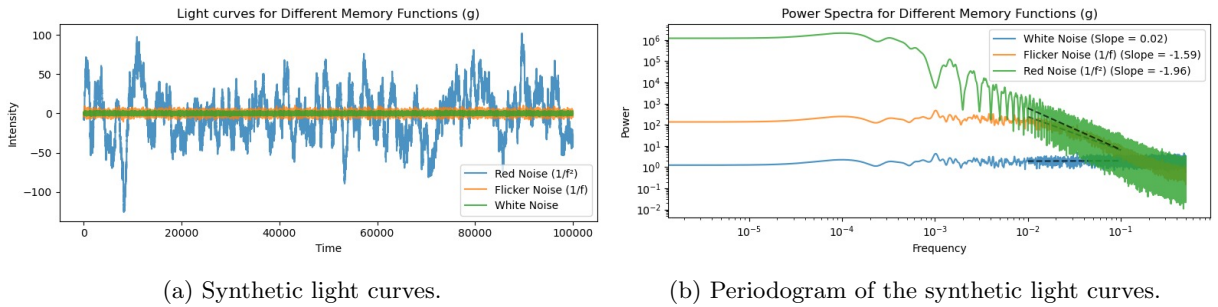(a) Synthetic light curves. (b) Periodogram of the synthetic light curves.

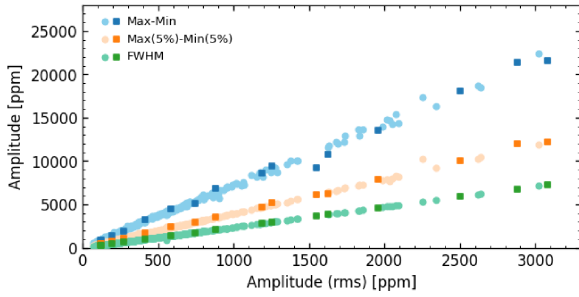Figure 3: Analysis of synthetic light curves.

3.2 RMS as a proxy for variability and flickering: validating RMS results from Merc, J. et al. (2024)

Calculating the Root Mean Square (RMS) of a light curve can shed some light onto the nature of a star's variability. In Merc, J. et al. (2024), it is used as a preliminary parameter for quantifying the amplitude of a star's brightness fluctuations. They employ several methods:
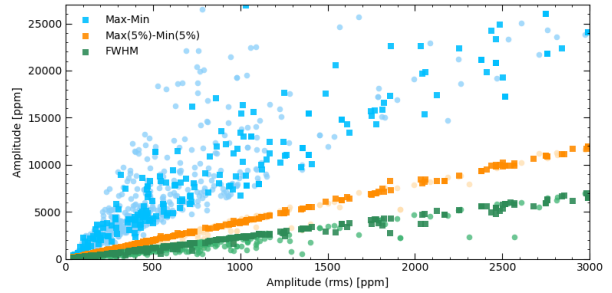
1. Peak-to-peak amplitude (as used in Zamanov et al. (2015)). Very susceptible to low frequency instrumental and natural fluctuations in the light curves.

2. Difference between the median of the top 5% highest and 5% lowest values.

3. Absolute RMS (as used in Uttley et al. (2005)). This refers to the classical definition of RMS, given by $\mathrm{RMS}\{x[n]\} = \sqrt{\frac{1}{N} \sum_n x^2[n]}$[11].

4. Full width at half maximum (FWHM) of a Gaussian fit to the collapsed points of the light curve (as used in Bruch (2021)). Also susceptible to low frequency instrumental and natural fluctuations in the light curves.

In order to validate the flickering detections in Merc, J. et al. (2024), we first need to validate their RMS results. We calculated the RMS values of all of our control sample AGB stars (Table 4), and the symbiotic and AGB stars used in Merc, J. et al. (2024) (Table 3 and Table 2). We also employed the same four methods. The RMS values calculated in this work are indeed in agreement with the work by Merc, J. et al. (2024) (see Figure 4). As shown in their work, the four methods for calculating the RMS are linearly dependent from one another. The peak-to-peak method (1) is the noisiest, reaching considerable spread in our results (light blue). This was to be expected, since the peak-to-peak method takes into account any of the low frequency trends that might have slipped through the smoothing filter.

---

[11]https://en.wikipedia.org/wiki/Root_mean_square

(a) RMS values from Merc, J. et al. (2024).

(b) RMS values from this work.

Figure 4: Comparison between RMS values. Known symbiotic stars in darker tones. Different methods vs. Absolute RMS (method 3): Peak-to-peak (blue), 5% extremes (orange), FWHM (green).

3.3 Negative high frequency slope as a proxy for flickering: validating slope results from Merc, J. et al. (2024)

Before attempting to recreate their results later in this section, we will explain in more depth the methodology used in Merc, J. et al. (2024). Apart from RMS, they used other tracers of flickering. Specifically, they searched for "red noise" (see Section 3.1), a negative slope in the high frequency region of the log-log plots of periodograms. Red noise is a common tracer for accretion disk emissions in not only symbiotic star research, but also for other types of stars (Dorn-Wallenstein et al. (2019)), or AGNs (Kraicheva et al. (1999)).

After cleaning out long-term trends using a 4σ clipping of outlier data and a Savitzky–Golay (SG) filter (Savitzky and Golay (1964)), they infer flickering using 3 techniques:

1. Measuring the power at 25 and 215 μHz in the periodogram.
2. Making two linear fits of the 20 - 1000 μHz region in the log-log periodogram plot: one at high frequencies ($>80\mu$Hz), and one at lower frequencies ($<80\mu$Hz). This is referred to later on in this section as *bilinear* fitting.
3. Estimating the RMS through 4 different methods.

They expect stars with flickering to have higher RMS, higher power at 215 μHz, and lower (i.e. more negative) high-frequency slope ($>80\mu$Hz) than single red giants with the same apparent magnitude. In Section 4, we will refer to the high frequency slope as *Slope2*, and to the low frequency slope as *Slope*. The frequency at which both linear fits separate is referred to as *Breakpoint*.

As seen in Figure 5, their results do hint at a clear difference between flickering symbiotic stars (orange) and single red giants (blue). Although some symbiotic stars do not deviate from the single red giant trend (blue curve), most are visibly separated in Figure 5a, Figure 5c and Figure 5d. Graph Figure 5b shows that no difference is expected for the low-frequency slope.

In Figure 5a, Figure 5c and Figure 5d, the object named RT Cru appears twice in the plots. That is because they noticed that the slope varied notably from sector to sector, suggesting the presence of an accretion disk exhibiting variable flickering behavior, with transitions between quiescent and active states. That is to be expected in flickering, since accretion disks are a naturally fluctuating phenomenon. Its intensity is strongly dependent on the amount of material falling in the accretion disk, which can vary greatly from year to year. That is why in our plots, shown in Section 3.3.1, we choose to show each sector as an individual point. When evaluating the results, it will be important to keep in mind that flickering stars might have sectors without flickering, due to its inherent variability.

3.3.1 Recreation of the results in Merc, J. et al. (2024): Fixed bilinear model

We now seek to validate whether symbiotic and isolated stars can be similarly separated based on their light curve properties in diagnostic diagrams created from the TESS and TESS-SPOC light curves. We already calculated RMS values in Section 3.2. In this subsection we show our results for the bilinear fittings of the periodograms. However, we encountered several problems. Firstly, as previously mentioned, they do not specify what stars they used as a control sample of isolated AGB stars, which forced us to select our own. Secondly, the specific method they use to calculate the high frequency slope is not explicitly shown in its totality. They do not specify if they constrained the separation between low and high frequency fittings, or up to what frequency they smoothed the light curve. Thus, we were forced to develop our own version of what we hoped was their intended method. We will present that method now.

The bilinear fitting consists on, as the name suggests, fitting 2 linear functions in the log-log periodogram that meet at a medium point, or "breakpoint". See Figure 6a for our method, and Figure 6b for the method from Merc, J. et al. (2024). In their work they mention that the typical frequency range for the breakpoint was 80μHz. When left free, the fitting algorithm preferred much higher frequencies for the breakpoint (around 1000μHz). In order to prevent that, and to keep the method as close as possible to that in Merc, J. et al. (2024), we forced the fitting to

(a) High-frequency slope vs. Magnitude.

(b) Low-frequency slope vs. Magnitude.

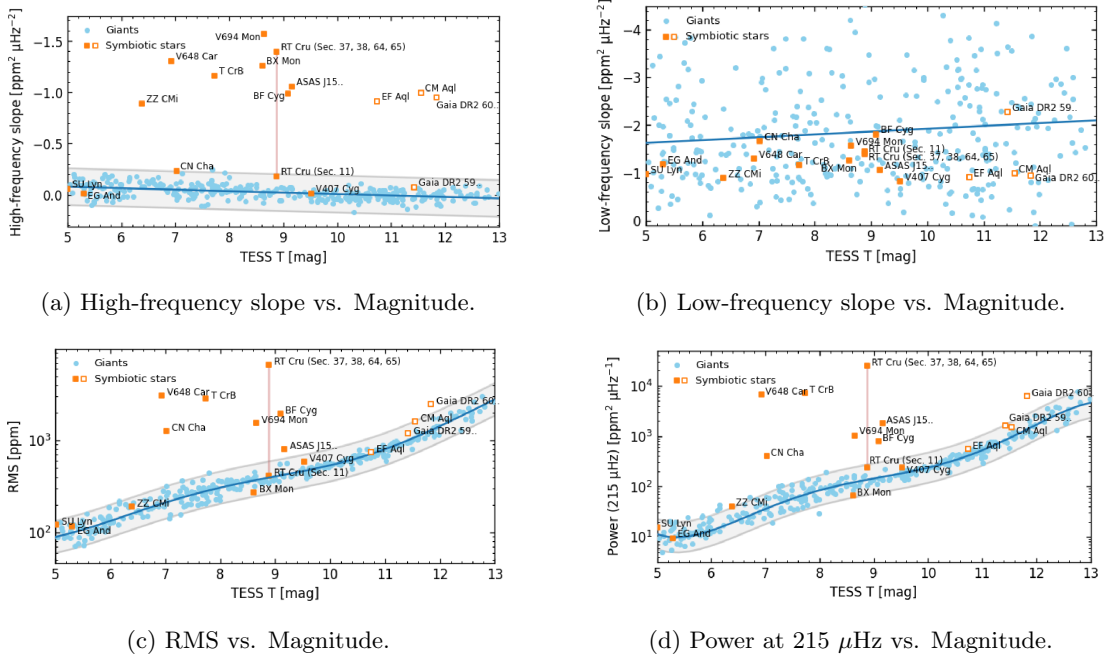(c) RMS vs. Magnitude.

(d) Power at 215 μHz vs. Magnitude.

Figure 5: Figures 11, 12, 13 and 14 from Merc, J. et al. (2024). Subset of studied symbiotic sources (orange squares) and red giants from the control sample (blue circles). The blue line shows the formal linear fit to the dependence for giants.

have a breakpoint between $60 - 100 \mu$Hz.

We remind the reader that we chose to represent each sector as a different point (Figure 6a), while in Merc, J. et al. (2024) they typically show the mean value of all sectors (Figure 6b). The precise sectors used can also differ from our work and theirs. We chose to do this to better illustrate the variability present in the flickering intensity, as several of the stars we studied had sectors with wildly different fittings, despite being the same object.

There are some other key differences between our method and theirs. First of all, they used Full Frame Images (FFI), instead of the SPOC light curves we used. That implies that they carried out their own instrumental corrections to the raw data from TESS, and defined their own custom apertures for each star. Not only would such a task fall outside of the time constrains for our work, it is also not explicitly shown how exactly they carried out this processing, so no effort was taken on our part to recreate this aspect of their analysis. Also, FFIs have higher cadences (fewer data points) than their SPOC counterparts, so in order to try and recreate as closely as possible the work in Merc, J. et al. (2024), we clipped our periodograms to the their same maximum frequency.

Secondly, they applied a strong smoothing filter to eliminate any of the low frequency trends. We did apply the same filter for RMS calculations, but we preferred to maintain low frequency trends in the linear fittings in fear of possibly eliminating true trends in the medium-frequency regime.
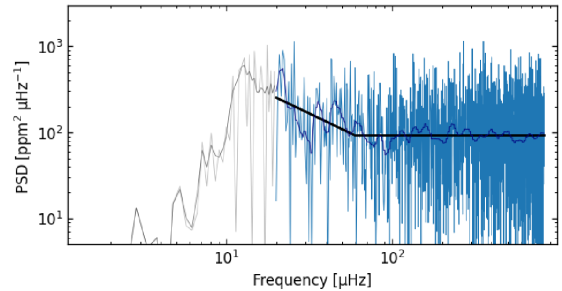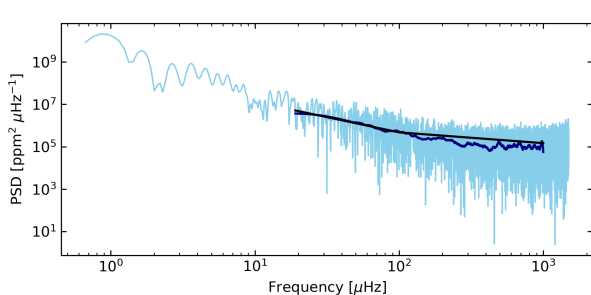
Applying the method described above to our sample of stars revealed that the results from Merc, J. et al. (2024) could not be exactly replicated. As seen in Figure 7 (which plots the high frequency slope with respect to the T magnitude), instead of a smooth trend of isolated AGB stars (blue), with flickering stars clearly deviating from them (orange), we obtained much noisier AGB stars (green). Although the slope values for the symbiotic stars were similar (the same stars as in Merc, J. et al. (2024) were used, see red squares in Figure 7), the fact that we cannot distinguish them from the control sample AGB stars makes their characterization much less clear than in their work.

4 Non-periodic variability: Alternative methods for flickering analysis

After not finding a definitive distinction between flickering and non-flickering objects by applying the methodology from Merc, J. et al. (2024), we attempted 2 alternative methods with the hope that they would make such a distinction much clearer. These include an improved bilinear model, modified in order to take full advantage of SPOC light curves' shorter cadence; and a non-linear model based on a pseudo-lorentzian function fitting, common in accretion disk emission characterization.

4.1 Free bilinear model

In an effort to improve upon the initial results from the fixed bilinear model, we designed a second variant of the method described in Merc, J. et al. (2024): the free bilinear model (see Figure 8a).

(a) Periodogram of the Sector 27 data of the red giant TIC 374859063. This work's fixed bilinear fitting model.

(b) Fig.10 in Merc, J. et al. (2024). Periodogram of the Sector 27 data of the red giant TIC 374859063.

Figure 6: Comparison between fixed bilinear models for the same star and sector. Raw periodogram in blue. Smoothed periodogram in darker blue. Linear fit in black.
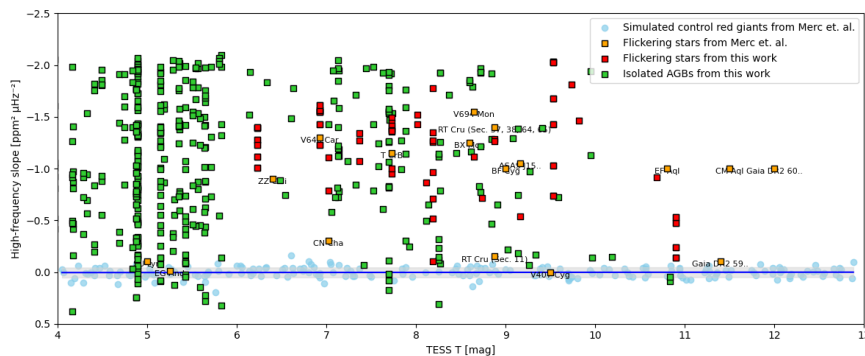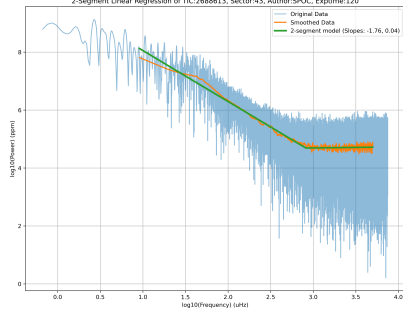

Figure 7: Comparison between Merc, J. et al. (2024) and this work (**fixed** bilinear model). The slope of at the high frequency regime ($> 80\mu Hz$) is plotted against the TESS magnitude. Simulated isolated red giants in blue (estimated values from Fig.12 in Merc, J. et al. (2024)), flickering sources from Merc, J. et al. (2024) in orange (one point per star, mean of all sectors), results from this work for the same flickering sources from Merc, J. et al. (2024) in red (one point by sector), the control sample of isolated AGB stars from this work in green.
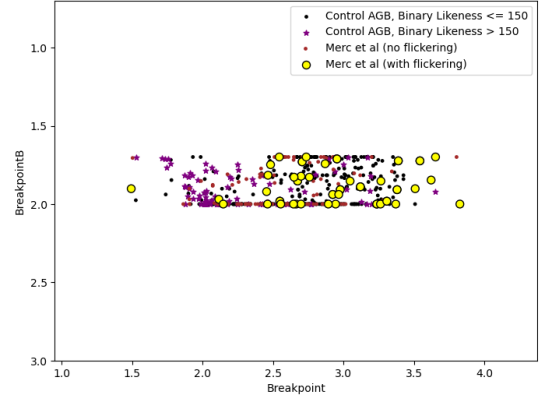
As in the fixed counterpart, the free bilinear model fits 2 linear functions to the 2 parts of the periodogram. This time however, we do not constrain the breakpoint frequency, allowing it to place itself at the optimal range, where the fitting's error is minimal. Hence "free" bilinear model. We also used the entire range of the periodogram, instead of clipping it to FFI ranges. This means we now have access to higher frequency regions of the periodogram. We sought to figure out if this higher frequency regime could facilitate the characterization of flickering, since it is a fundamentally fast-changing phenomenon. We also intended to find out if some of the flickering detections in Merc, J. et al. (2024) might actually be false positives, wrongly identified due to the restricted spectrum of frequencies available in FFI.

Applying this second method to our sample did not allow us to differentiate flickering stars from non-flickering stars either (see Figure 9). We did see the effects of freeing the breakpoint position. In Figure 8b (comparison between breakpoints in the free and fixed models) it is easy to see that constraining the breakpoint to $60 - 80\mu Hz$ was forcing the model to avoid the best fit in most sectors. Figure 8c (high frequency slope in the fixed model vs. the free breakpoint) shows that both of the plotted variables are coupled, most likely because forcing the breakpoint to remain at $80\mu Hz$ ($log_{10}(80) \approx 1.9$) was also leaving as "high frequency region" data with a high slope that would have otherwise been included in the "low frequency region", hence increasing the hi-fi slope for higher breakpoint frequencies.
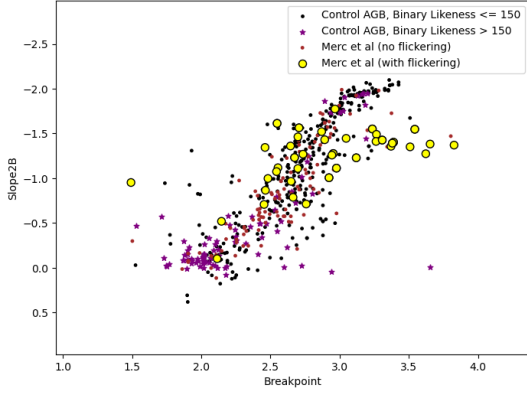
Lastly, in Figure 8d (high frequency slopes in the fixed (Slope2B) and free (Slope2) bilinear models) one can see that for values of Slope2B closer to 0, Slope2 is much more clumped up around 0. On the other hand, for values of Slope2B further from 0, Slope2 spreads through more values. This is because the free model is much better at detecting the transition between the slope and the white instrumental noise (see Figure 8a), resulting in a value close to 0 for the hi-fi slope (that fits exclusively the instrumental white noise). This does not happen in the fixed model, since having the breakpoint constrained to lower frequencies does not allow for the white noise to be isolated to the hi-fi slope. This might have been an intended result of Merc, J. et al. (2024). Nonetheless, the clear distinction between their flickering detections and control sample is still not easily visible in our results, as seen in the plots of the high (Figure 9a) and low (Figure 9b) frequency slopes.
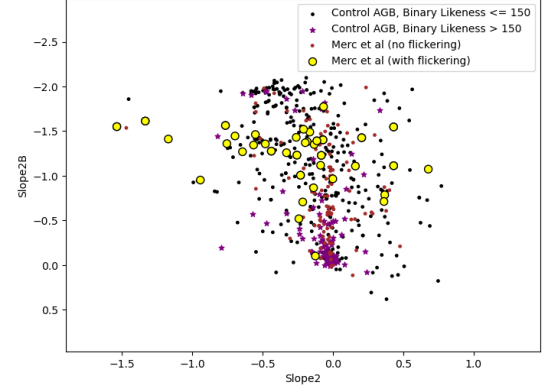
(a) Free bilinear fit of TIC 2688613 (sector 43). Raw (blue), smoothed (orange), fit (green).

(b) Breakpoint comparison: free (Breakpoint) vs. fixed (BreakpointB) model.
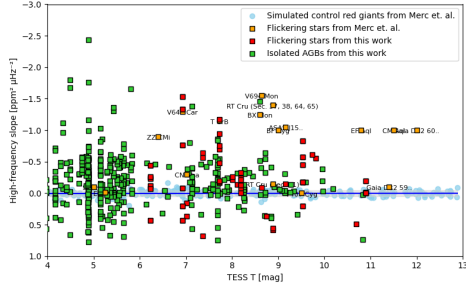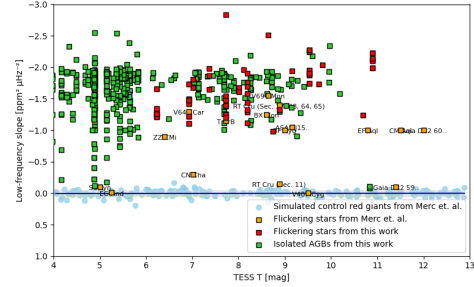

(c) Free Breakpoint vs. fixed model slope.

(d) Slope comparison: fixed (Slope2B) vs. free (Slope2) model.

Figure 8: Free bilinear model analysis. (a) Example periodogram fit; (b-d) Parameter comparisons showing flickering sources (yellow), non-flickering (brown), and control AGB stars (black/purple by binarity likelihood).

(a) High frequency Slope2 ($> 80\mu$Hz) against TESS magnitude.

(b) Low frequency Slope ($< 80\mu$Hz) against TESS magnitude.

Figure 9: Comparison between Merc, J. et al. (2024) and this work (**free** bilinear model). The slope is plotted against the TESS magnitude. Simulated isolated red giants in blue (estimated values from Fig.12 in Merc, J. et al. (2024)), flickering sources from Merc, J. et al. (2024) in orange (one point per star, mean of all sectors), results from this work for the same flickering sources from Merc, J. et al. (2024) in red (one point by sector), the control sample of isolated AGB stars from this work in green.

4.2 Alternative method: non-linear model

Lastly, we tried a non-linear fitting model based on other analysis of flickering in the literature. We found that a lot of the research being made on the topic of flickering detection (as in Kourniotis et al. (2025)) used pseudo-lorentzian functions, as opposed to linear ones. This particular method has not yet been used for symbiotic stars, however. The particular equation used in our work was:

$$P(\nu) = B + \frac{A}{1 + (2\pi\tau\nu)^\gamma} \tag{1}$$

where the power of the periodogram ($P(\nu)$) is described by parameters A, B, τ and γ. ν is the frequency. An example of this fit can be seen in Figure 10a. Next we offer simple considerations for the physical meaning behind each parameter. Note that the function takes meaning when seen in log-log plots.
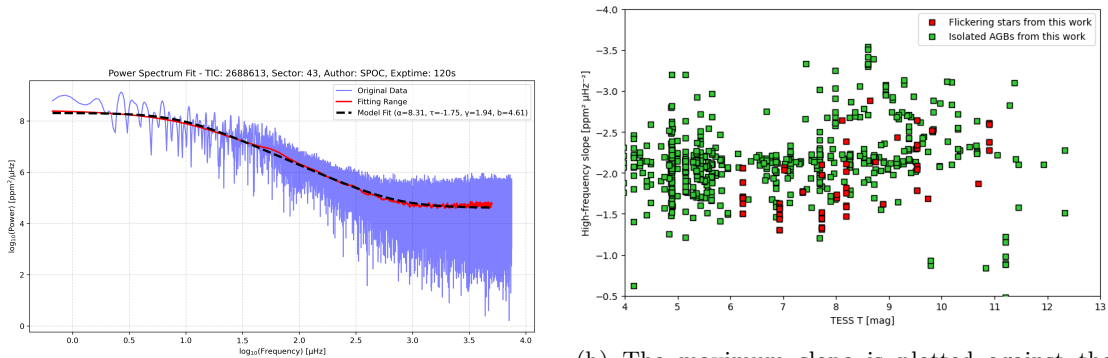
- B can be thought of as the minimum noise level, or the base intensity of the highest frequencies, where instrumental white noise dominates.
- A can be thought of as the maximum natural signal intensity, reached at the lowest frequencies.
- τ can be thought of as the inverse of the frequency where the downwards trend begins, which is correlated with the temporal scale at which flickering would be occurring (as seen in Degott et al. (2025)). Technically, it represents the period at which half of the maximum intensity is achieved.
- γ can be thought of as the steepness of the descend at frequency τ^{-1}.

In Degott et al. (2025) they used this same technique for analyzing active low-mass stars. They used the parameter τ as a proxy for rotational modulation variability (i.e. the variability resulting from sunspots periodically entering and leaving our line of sight). They found that $log_{10}(\tau[\mathrm{days}])$ had typical values between -0.3 and 0.3. They also found parameter A to be correlated to stellar activity.

In Ma et al. (2024) they also used this non-linear method for blue supergiant stars. They found that γ was typically between values of 2 to 6, while $log_{10}(\tau[\mathrm{days}])$ was between values of -1.3 and -0.6.

In our case, we should expect lower values for τ (from hours to minutes, $log_{10}(\tau[\mathrm{days}]) \approx -2$), since flickering is a fast-pace phenomenon that should introduce the slope at high frequencies. We should also expect γ to be high (around 2), since it should be coupled to the slope measured in the bilinear models. As seen in Figure 11, we obtained results with values for $log_{10}(\tau[\mathrm{days}])$ ranging from 0 to -1, not as high frequency as the blue supergiants, but definitely more high frequency than the low-mass stars. For γ we obtained values between 1.5 and 2.5. However, we observed that confirmed flickering sources from Merc, J. et al. (2024) had lower γ values, instead of higher. This will be expanded upon in Section 5.

Figure 10b shows the maximum slope (max_slope) obtained with the non-linear model against the TESS magnitudes. No clear deviation from flickering and non-flickering sources can be seen here either. In this case (the non-linear model), the slope was calculated by analytically obtaining the derivative of the model function, and then obtaining the maximum slope value. In Section 5 we will explore in more detail if these non-linear parameters offer any advantage over linear fittings when differentiating flickering from non-flickering stars.

(a) Example of a non-linear fit of TIC 2688613, sector 43, using a SPOC light curve with a cadence of 120 seconds. Raw periodogram in blue. Smoothed periodogram in red. Linear fit in black.

(b) The maximum slope is plotted against the TESS magnitude. Results from this work for the same flickering sources from Merc, J. et al. (2024) in red (one point by sector), the control sample of isolated AGB stars from this work in green.

Figure 10: Non-linear model.

5 The search for flickering: Results

In this section we will show the trends and correlations we found in the different results from prior sections. These include the four RMS calculations and the three different fitting models.

We remind the reader that our control sample of isolated AGB stars has a threshold value for the Binary Likeness parameter of 150 or lower. Although stars with Binary Likeness > 150 are also plotted, they are not to be mistaken with the control sample. We include them in order to maximize potential flickering detections, since our selection method via UV excess could prove to be useful for binarity detection. As mentioned in prior sections, we also
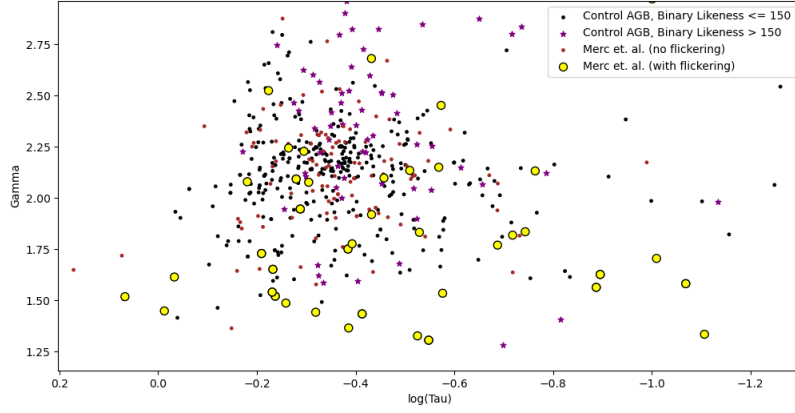
Figure 11: γ values against $log_{10}(\tau[days])$ values. Results from this work for the detected flickering sources from Merc, J. et al. (2024) are in yellow, non-flickering sources from Merc, J. et al. (2024) are in brown, the control sample of isolated AGB stars from this work is in black (Binary Likeness $\leq$ 150) and purple (Binary Likeness > 150).

used CROWDSAP> 0.95 as our threshold for minimum contamination. Only stars with $T_{mag} < 4$, and SPOC or TESS-SPOC light curves available, are plotted in this section.

The color coding is the same in all scatter plots: results from this work for the detected flickering sources from Merc, J. et al. (2024) are in yellow, non-flickering sources from Merc, J. et al. (2024) are in brown, the control sample of isolated AGB stars from this work is in black (Binary Likeness $\leq$ 150) and purple (Binary Likeness > 150), stars from the Variability Catalog of Stars are shown as red crosses, objects from Oomen et al. (2018) (van Winkle objects) are shown as empty orange circles, x-AGB stars are shown as green crosses, and WD with IR excess are shown as empty blue circles.

The abundance of catalogs and sectors might make some of the plots somewhat messy and difficult to follow. When a more detailed view of some particular correlation is needed, isolated plots or histograms will be shown to ease readability. More plots are available at this GitHub page.

5.1 Magnitude correlations

First we explore the correlation between the TESS magnitude and the RMS or γ non-linear parameter. We still seek to validate the results from Merc, J. et al. (2024), in particular, their results for the RMS vs. Magnitude plot (see Figure 5c for their results, Figure 12a for ours). As discussed in Section 3.2, the same trend for the minimum RMS for a given TESS magnitude is still observed. Some flickering sources from Merc, J. et al. (2024) do seem to have higher RMS than isolated stars, but others remain at the lower trend that Merc, J. et al. (2024) associates with the control sample of red giants.

At higher brightness (lower magnitudes) it is hard to conclude anything. Objects in that region appear to fluctuate a lot more in RMS (vertical strings of points close together are the result of different sectors of the same object having contiguous RMS values). There does not seem to be a trend at low magnitudes, and since there are no flickering stars from Merc, J. et al. (2024) in that region, no direct comparison can be made. This might be due to the data being faulty (perhaps our threshold for minimum magnitude was not high enough, and TESS saturates at fainter brightness). Or perhaps we are observing at low magnitudes stellar types with intrinsically higher variability from sector to sector that at higher magnitudes might be invisible due to their distance. This seems to be the case for x-AGB stars (green crosses), which are much more present at low magnitudes, suggesting an observational bias.

Assuming a high RMS is indeed a tracer for flickering at the range of magnitudes at which flickering stars from Merc, J. et al. (2024) can be found (around 7 to 9 magnitudes), we suggest the objects in Table 9 as candidates for flickering.

Secondly, in Figure 12b we show γ vs. the TESS magnitude. In this figure we can clearly see distinctions between catalogs, made much clearer because of the different brightness levels. Again, x-AGB stars seem to populate the lower magnitudes, while AGB stars from our control sample with Binarity Likeness > 150 seem to populate the higher magnitudes. Most notably, post-AGB objects from the Variability Catalog of Stars (Fetherolf et al. (2023)) seem to be spread out through all magnitudes and have systematically higher γ values than the rest of catalogs (see Figure 16 for mean values of γ).

(a) $log_{10}(RMS_{abs})$ vs. the TESS magnitude.

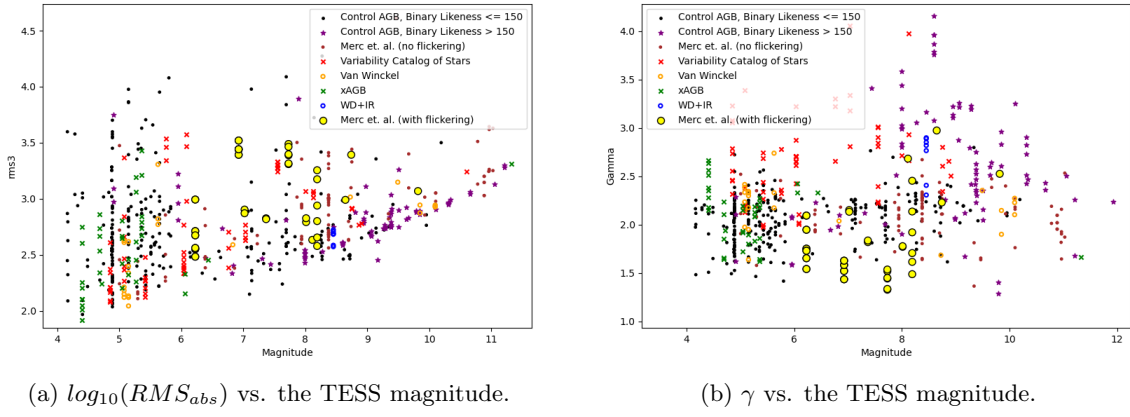

(b) γ vs. the TESS magnitude.

Figure 12: RMS plots.

Table 9: Stellar parameters for flickering candidates between 7 and 9 T_{mag} based on RMS values. Known flickering symbiotic stars from Merc, J. et al. (2024) have been excluded.

TIC ID	Magnitude	Catalog	Sectors
4385592	9.50	Isolated AGB	72
422989548	7.69	Isolated AGB	17, 25
58227898	9.13	Isolated AGB	70
397514892	8.25	Isolated AGB	78
120504920	8.14	Isolated AGB	69
129077819	8.84	Isolated AGB	67
129684571	7.88	Isolated AGB	57
264248402	8.27	Isolated AGB	56
264413925	7.52	Isolated AGB	72
316417053	7.13	Isolated AGB	75
388775434	9.66	Merc et. al. (no flickering)	82
333326188	8.74	Merc et. al. (no flickering)	80
282619434	7.86	Merc et. al. (no flickering)	81
237100139	8.37	Merc et. al. (no flickering)	74, 75, 84
83299618	7.94	Merc et. al. (no flickering)	75
6348255	9.46	Merc et. al. (no flickering)	80
337886863	7.55	Variability Catalog of Stars	16, 17, 18, 24, 57, 58, 77, 84

5.2   Noise parameters

Noise is strongly related to flickering. In fact, an important challenge researchers face when attempting to infer the presence of flickering is differentiating it from other sources of noise. Thus, it is important to understand how we have parametrized noise in this work, as it might prove a useful resource when attempting to measure flickering. In Figure 13 we plot several noise-related correlations. In Figure 13a we can see that the B parameter in the non-linear model (which quantifies the minimum noise level at the highest frequencies) is strongly related to the absolute RMS, as was to be expected. This type of plot might be useful for flickering detection, since a high RMS but low B might indicate that the star possesses an intense source of intrinsic noise that does not originate from instrumental noise. We can also see in Figure 13d that the higher the magnitude value, the higher the minimum B value, as was to be expected (observational biases skew the stars at low brightness levels towards more variable and luminous stellar types).

During the analysis, when considering if γ was a good tracer of the slope of the periodogram, we suspected that the values of γ might be influenced by the instrumental noise of the light curve. In other words, we feared γ was getting coupled to the difference between the maximum signal intensity (A) and the minimum floor-level white noise (B), meaning that instead of measuring the slope flickering might produce, it was in fact measuring the slope generated by the contrast difference between the natural signal and the artificial noise, which is highly dependent on the apparent magnitude. In order to quantify this coupling, we show in Figure 13b γ against the difference between $log_{10}(A)$ and $log_{10}(B)$. The plot shows that no notable coupling can be measured, thus making γ a valid tracer of the slope. The same result can be seen in Figure 13c, this time with respect to magnitude.
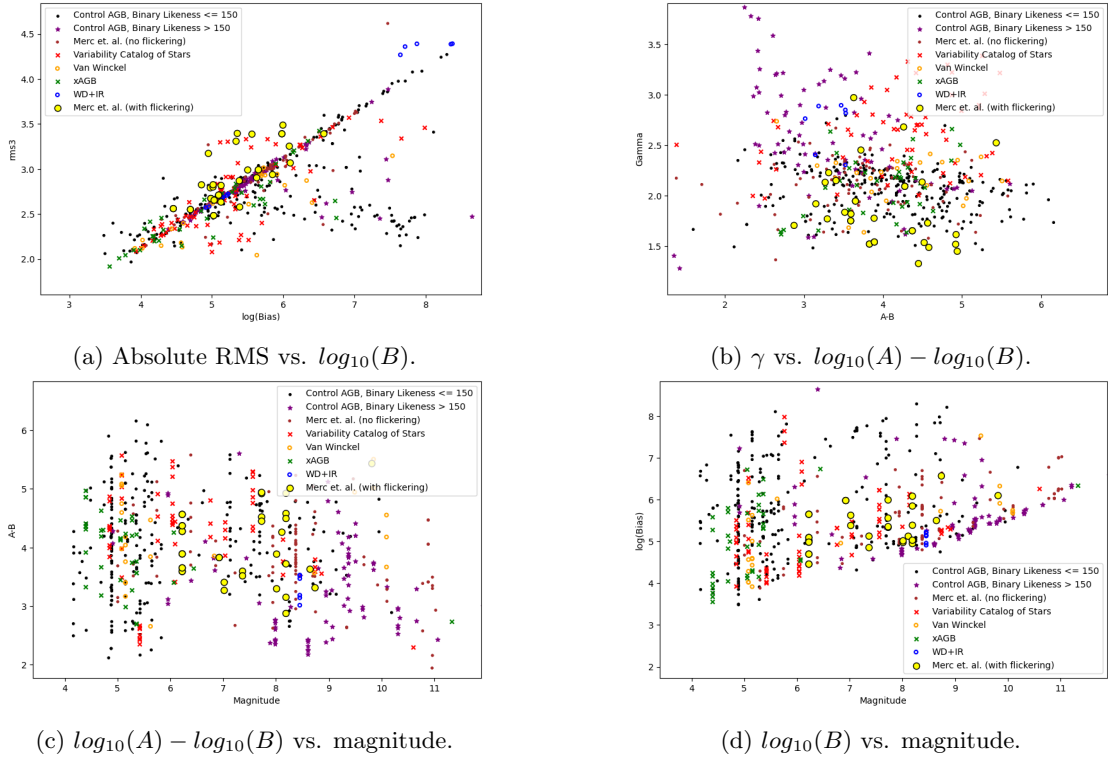
(a) Absolute RMS vs. $log_{10}(B)$.

(b) γ vs. $log_{10}(A) - log_{10}(B)$.

(c) $log_{10}(A) - log_{10}(B)$ vs. magnitude.

(d) $log_{10}(B)$ vs. magnitude.

Figure 13: Several noise parameter correlations.

5.3 Parameter γ

We now show the general trends observed for the non-linear parameter γ. As previously mentioned in Section 3.5, flickering sources from Merc, J. et al. (2024) gravitated towards lower γ values, instead of higher values (see Figure 14). It was first thought that this might mean that the γ parameter was, in fact, not coupled to the slope from the bilinear models. However, Figure 15a shows that γ and the slope calculated in the non-linear model (max_slope) are indeed correlated.

Although not as clearly as the slope vs. magnitude graphs in Merc, J. et al. (2024) (see Figure 5), the γ parameter does offer some differentiation between flickering and non-flickering stars. Figure 16 shows the same data as Figure 14, but separated by catalogs. The area inside the white ellipses contains around 50% of the data points, and can be thought of as the spread of the distribution. One can clearly see that the known flickering objects (lower left) have considerable higher spread, even when taking into account the difference in data points. As previously mentioned, γ has systematically lower values in flickering stars, with a mean of 1.79 with respect to 2.10.

Figure 16 also shows that both the post-AGB stars from the Variability Catalog of Stars (Fetherolf et al. (2023)) and the WD-IR catalog stars have significantly higher γ values, and somewhat lower τ values. Examples for light curves and periodograms for all of this types of stars have been included in the Appendix.

Figure 15b, Figure 15c and Figure 15d show some correlations between γ and the bilinear models. One can see that flickering stars from Merc, J. et al. (2024) have lower low frequency slopes, but higher high frequency (hi-fi) slopes.
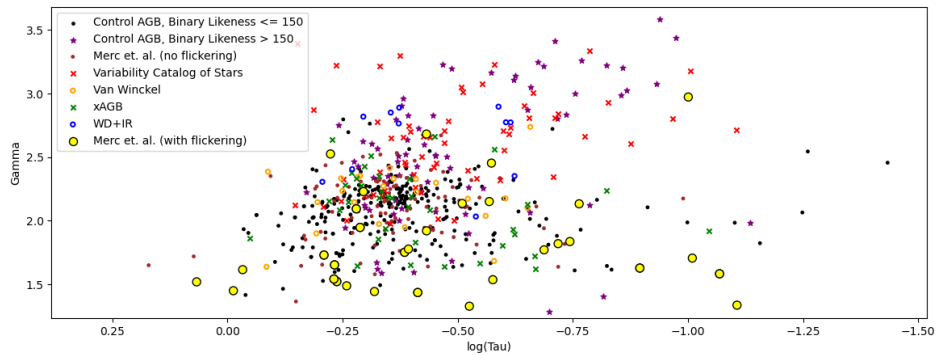

Figure 14: γ values against $log_{10}(\tau[\text{days}])$ values.
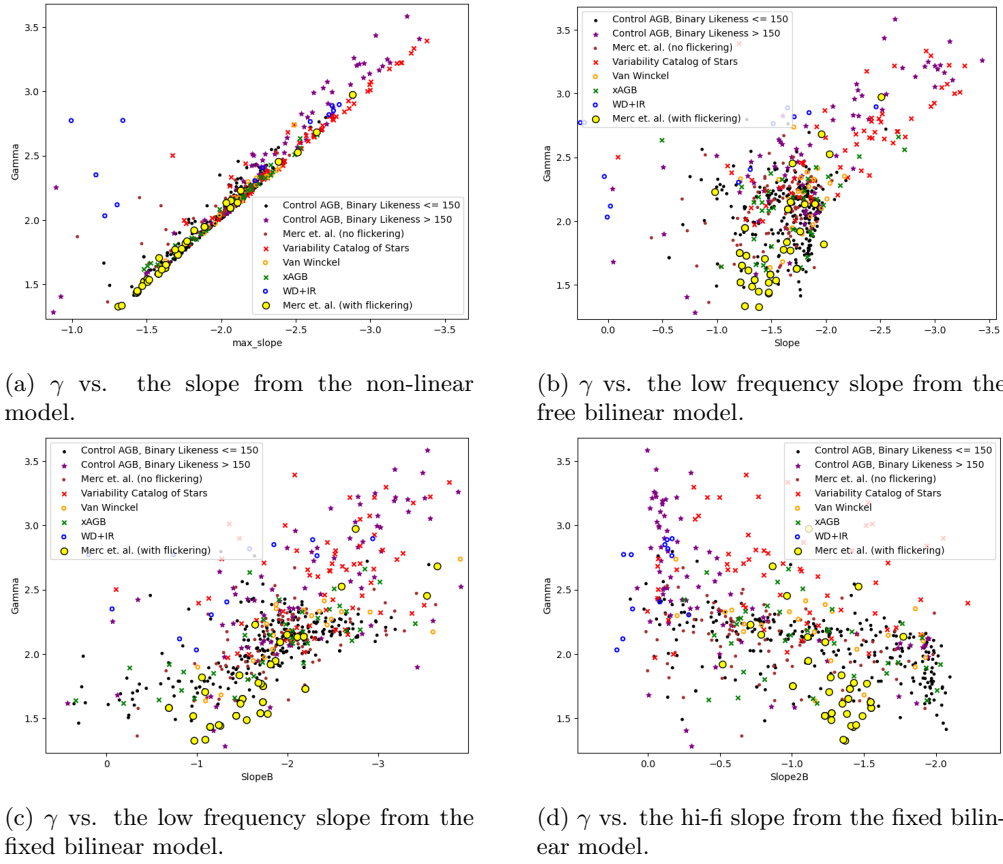
(a) γ vs. the slope from the non-linear model.

(b) γ vs. the low frequency slope from the free bilinear model.

(c) γ vs. the low frequency slope from the fixed bilinear model.

(d) γ vs. the hi-fi slope from the fixed bilinear model.
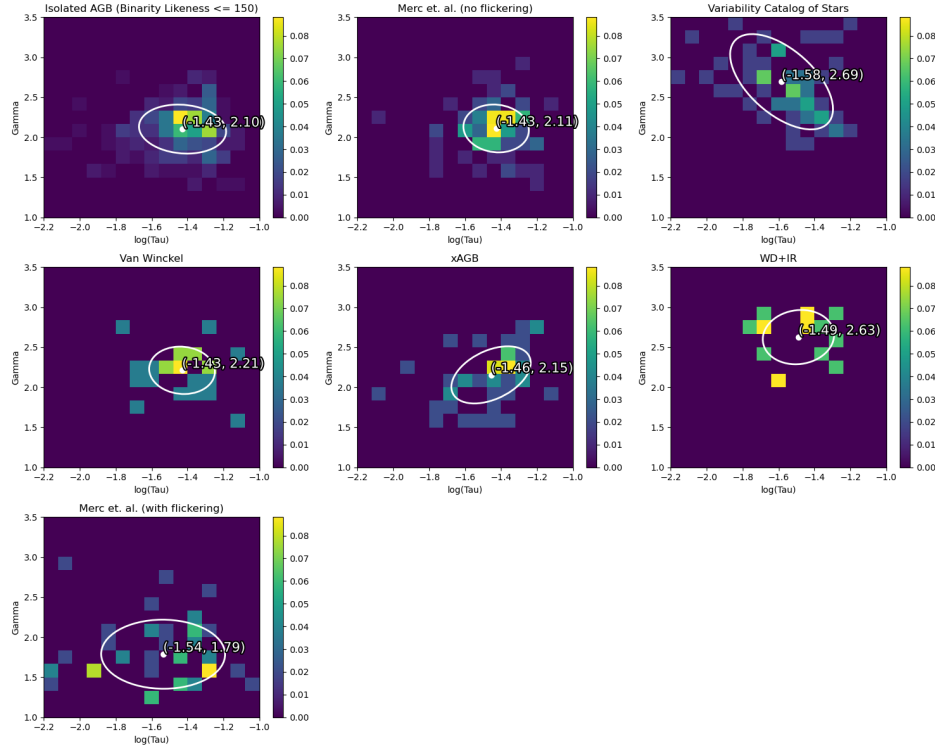
Figure 15: Several γ correlations.

Figure 16: γ values against $log_{10}(\tau[\text{days}])$ values for all catalogs. The white dot shows the mean value. The white ellipse surrounds an area containing approximately 50% of the data points.

6 Periodic variability: pilot study

Periodic signal detection was not a priority in this work, but it was nonetheless a secondary goal. In this section we present a brief overview of the results we obtained for the characterization of periodic variability in the catalogs studied in this work. In Figure 17 we show the frequency of maximum power (in days^{-1}) with respect to magnitude. Most stars had maximum frequencies around 0.1 days. This is no coincidence. As mentioned in Section 2.3.2, downlink time can introduce artificial peaks at $f = 1/13$ days$^{-1} \approx 0.1$. TESS light curves require elaborate data analysis in order to get around this issue, which goes beyond the scope of this work. Even though we cannot show quality results for periodic variability measurements in the frequency region dominated by downlink artifacts, we did detect in the periodograms known binaries (see Figure 18a for a periodogram of the spectroscopic binary CRTS J131559.4-370018, which displays an intense peak at 2.6 days^{-1}) and solar-like oscillations (see Figure 18b, which displays a gaussian bump in frequency at the middle of the periodogram, as seen in the objects studied in Zhou et al. (2024)).
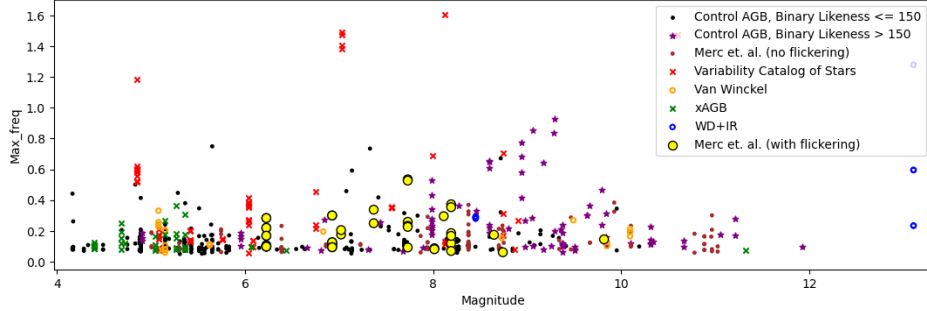

Figure 17: Frequency of maximum power (in days^{-1}) with respect to magnitude. Value obtained from the linear low frequency periodograms (see Figure 1e).

(a) Example of a periodogram of binary system CRTS J131559.4-370018. Notice the peak at $log_{10}(F) = 1.7$. A folded light curve of this object for that frequency can be found at GitHub page.

(b) Example of a periodogram of a star with solar-like oscillations. Notice the gaussian bump at $log_{10}(F) = 1.7$.
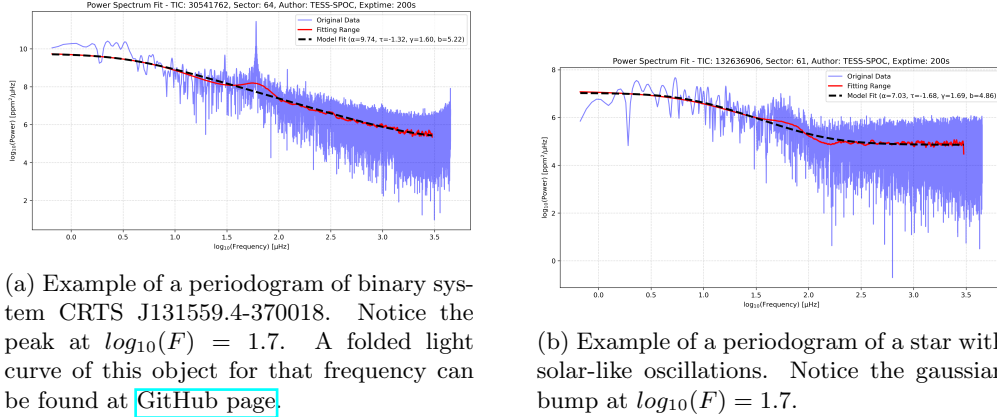
Figure 18: Periodograms of some of the binaries and solar-like oscillations found.

7 Conclusions

The goal of this work was to characterize variability in AGB stars using TESS data. More specifically, this work has analyzed the possibility of using TESS data for the detection of high frequency stochastic red noise (flickering). We sought to take advantage of the high quality, short cadence, 27 day-long light curves TESS has made available for previously unexplored AGB, post-AGB, x-AGB and WD stars. By detecting flickering in these objects, binarity can be inferred and analyzed in detail in follow-up studies. The overarching motivation behind this study was to better understand how binarity might be the culprit behind the morphology of pPN, potential successors of those AGB-stars which exhibit flickering.

We closely followed the steps of Merc, J. et al. (2024) for the initial flickering detection methodology. Since their results could not be exactly replicated (particularly the clear separation between flickering and isolated stars), we expanded upon their work by introducing two new methods of analysis: the free bilinear and non-linear models. We proposed a list of flickering candidates (see Table 9) based on RMS values. We also found that some separation between stellar catalogs was achieved with the non-linear fitting parameter γ: flickering sources clustered at lower values ($\gamma < 2.0$), while isolated AGB stars exhibited systematically higher values. Some general characterization was

also found for post-AGB stars from the Variability Catalog of Stars (Fetherolf et al. (2023)) and WD+IR (Farihi et al. (2025)), with systematically higher γ and lower τ values than isolated AGB stars.

One of the main challenges we faced during our research was figuring out if our selection of objects for the control sample of AGB stars was appropriate. Since one of our primary goals was to isolate the effects of flickering on the fitting parameters, having a suitable selection of control stars confirmed not to have any flickering was of extreme importance. In Figure 19 we show the absolute RMS values of all the AGB stars considered for the control sample with respect to magnitude. The color coding indicates the Binary Likeness, ranging from blue (unlikely) to red (likely). We feared our method would deprecate stars based on magnitude, instead of actual binary likelihood. There seemed to be some bias towards higher brightness values, but overall, a homogeneous range of magnitudes was achieved.

However, it is undeniable that some magnitude-dependent biases were introduced through the control sample into the results (see the spread at high brightness values in Figure 19). We strongly recommend researchers carrying out similar analysis to refine a good control sample independent of brightness with which to properly compare flickering candidates.

A study of the periodic variability of all the stars was also attempted, but the results were greatly contaminated by downlink gaps in the light curves. Binaries and solar-like oscillations were observed.

Ultimately, this work has shown both the potential and limitations of using TESS data for flickering detection. The high quality, short cadence, high area coverage of TESS makes it suitable for this kind of research. However, the coarse pixel size and the redder passband limit the precision with which flickering detections might ultimately be made. Future missions, such as PLATO or other light curve oriented surveys, might fill in the gaps of TESS, and allow for a precise and exact characterization of how binarity shapes late-stage stellar evolution.
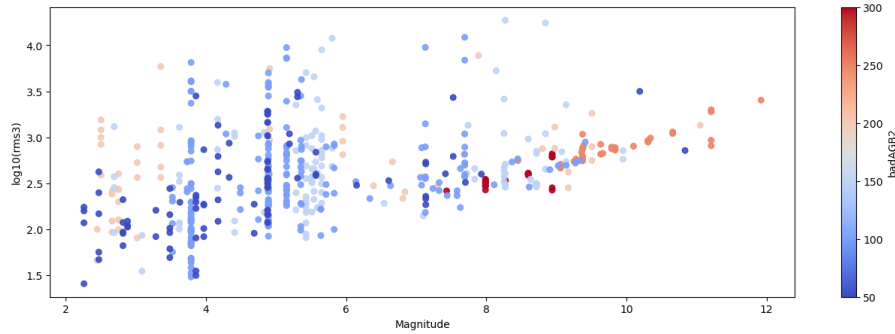

Figure 19: Comparison between the AGB stars considered for the control sample. Blue indicates low Binary Likeness, while red high Binary Likeness.

References

A. Aller, J. Lillo-Box, D. Jones, L. F. Miranda, and S. Barceló Forteza. Planetary nebulae seen with TESS: Discovery of new binary central star candidates from Cycle 1. , 635:A128, Mar. 2020. doi: 10.1051/0004-6361/201937118.

A. Bruch. Flickering in cataclysmic variables : its properties and origins. , 266:237–265, Dec. 1992.

A. Bruch. A comparative study of the strength of flickering in cataclysmic variables. , 503(1):953–971, May 2021. doi: 10.1093/mnras/stab516.

D. Chakrabarty and P. Roche. The symbiotic neutron star binary gx 1+4/v2116 ophiuchi. *The Astrophysical Journal*, 489(1):254–271, Nov. 1997. ISSN 1538-4357. doi: 10.1086/304779. URL http://dx.doi.org/10.1086/304779.

L. Degott, F. Baudin, R. Samadi, B. Perri, and C. Pinçon. Activity of low-mass stars in the light of spot signature in the fourier domain. *Astronomy amp; Astrophysics*, 696:A41, Apr. 2025. ISSN 1432-0746. doi: 10.1051/0004-6361/202451205. URL http://dx.doi.org/10.1051/0004-6361/202451205.

T. Z. Dorn-Wallenstein, E. M. Levesque, and J. R. A. Davenport. Short-term Variability of Evolved Massive Stars with TESS. , 878(2):155, June 2019. doi: 10.3847/1538-4357/ab223f.

J. Farihi, K. Y. L. Su, C. Melis, S. J. Kenyon, A. Swan, S. Redfield, M. C. Wyatt, and J. H. Debes. Subtle and spectacular: Diverse white dwarf debris disks revealed by jwst, 2025. URL https://arxiv.org/abs/2501.18338.

T. Fetherolf, J. Pepper, E. Simpson, S. R. Kane, T. Močnik, J. E. English, V. Antoci, D. Huber, J. M. Jenkins, K. Stassun, J. D. Twicken, R. Vanderspek, and J. N. Winn. Variability catalog of stars observed during the tess prime mission. *The Astrophysical Journal Supplement Series*, 268(1):4, aug 2023. doi: 10.3847/1538-4365/acdee5. URL https://dx.doi.org/10.3847/1538-4365/acdee5.

M. A. Guerrero, R. Montez, R. Ortiz, J. A. Toalá, and J. H. Kastner. Asymptotic giant branch stars in the eROSITA-DE eRASS1 catalog. , 689:A62, Sept. 2024. doi: 10.1051/0004-6361/202450155.

R. Kippenhahn, A. Weigert, and A. Weiss. *Evolution on the Asymptotic Giant Branch*, pages 417–438. Springer Berlin Heidelberg, Berlin, Heidelberg, 2012. ISBN 978-3-642-30304-3. doi: 10.1007/978-3-642-30304-3_34. URL https://doi.org/10.1007/978-3-642-30304-3_34.

M. Kourniotis, L. S. Cidale, M. Kraus, M. A. Ruiz Diaz, and A. Alberici Adam. Variability of galactic blue supergiants observed with tess. *Astronomy amp; Astrophysics*, 697:A152, May 2025. ISSN 1432-0746. doi: 10.1051/0004-6361/202452360. URL http://dx.doi.org/10.1051/0004-6361/202452360.

Z. Kraicheva, V. Stanishev, V. Genkov, and L. Iliev. TT Arietis: 1985-1999 accretion disc behaviour. , 351:607–618, Nov. 1999.

Lightkurve Collaboration, J. V. d. M. Cardoso, C. Hedges, M. Gully-Santiago, N. Saunders, A. M. Cody, T. Barclay, O. Hall, S. Sagear, E. Turtelboom, J. Zhang, A. Tzanidakis, K. Mighell, J. Coughlin, K. Bell, Z. Berta-Thompson, P. Williams, J. Dotson, and G. Barentsen. Lightkurve: Kepler and TESS time series analysis in Python. Astrophysics Source Code Library, Dec. 2018.

L. Ma, C. Johnston, E. P. Bellinger, and S. E. de Mink. Variability of blue supergiants in the lmc with tess. *The Astrophysical Journal*, 966(2):196, may 2024. doi: 10.3847/1538-4357/ad38bc. URL https://dx.doi.org/10.3847/1538-4357/ad38bc.

Merc, J., Beck, P. G., Mathur, S., and García, R. A. Accretion-induced flickering variability among symbiotic stars from space photometry with nasa tess. *AA*, 683:A84, 2024. doi: 10.1051/0004-6361/202348116. URL https://doi.org/10.1051/0004-6361/202348116.

G.-M. Oomen, H. Van Winckel, O. Pols, G. Nelemans, A. Escorza, R. Manick, D. Kamath, and C. Waelkens. Orbital properties of binary post-agb stars. *Astronomy amp; Astrophysics*, 620:A85, Dec. 2018. ISSN 1432-0746. doi: 10.1051/0004-6361/201833816. URL http://dx.doi.org/10.1051/0004-6361/201833816.

R. Ortiz and M. A. Guerrero. Ultraviolet emission from main-sequence companions of agb stars. *Monthly Notices of the Royal Astronomical Society*, 461(3):3036–3046, June 2016. ISSN 1365-2966. doi: 10.1093/mnras/stw1547. URL http://dx.doi.org/10.1093/mnras/stw1547.

R. Sahai, J. D. Neill, A. Gil de Paz, and C. Sánchez Contreras. Strong variable ultraviolet emission from y gem: Accretion activity in an asymptotic giant branch star with a binary companion? *The Astrophysical Journal*, 740 (2):L39, Sept. 2011. ISSN 2041-8213. doi: 10.1088/2041-8205/740/2/l39. URL http://dx.doi.org/10.1088/2041-8205/740/2/L39.

R. Sahai, C. S. Contreras, A. S. Mangan, J. Sanz-Forcada, C. Muthumariappan, and M. J. Claussen. Binarity and accretion in agb stars: Hst/stis observations of uv flickering in y gem. *The Astrophysical Journal*, 860(2):105, jun 2018. doi: 10.3847/1538-4357/aac3d7. URL https://dx.doi.org/10.3847/1538-4357/aac3d7.

A. Savitzky and M. J. E. Golay. Smoothing and differentiation of data by simplified least squares procedures. *Analytical Chemistry*, 36:1627–1639, Jan. 1964. doi: 10.1021/ac60214a047.

K.-W. Suh. A new catalog of asymptotic giant branch stars in our galaxy. *The Astrophysical Journal Supplement Series*, 256(2):43, Oct. 2021. ISSN 1538-4365. doi: 10.3847/1538-4365/ac1274. URL http://dx.doi.org/10.3847/1538-4365/ac1274.

M. Sun, S. Levina, S. Gossage, V. Kalogera, E. M. Leiner, A. M. Geller, and Z. Doctor. Wind roche-lobe overflow in low-mass binaries: Exploring the origin of rapidly rotating blue lurkers, 2024. URL https://arxiv.org/abs/2311.07528.

J. A. Toalá, O. González-Martín, A. Sacchi, and D. A. Vasquez-Torres. The x-ray rise and fall of the symbiotic recurrent nova system t crb. *Monthly Notices of the Royal Astronomical Society*, 532(2):1421–1433, 07 2024. ISSN 0035-8711. doi: 10.1093/mnras/stae1579. URL https://doi.org/10.1093/mnras/stae1579.

P. Uttley, I. M. McHardy, and S. Vaughan. Non-linear X-ray variability in X-ray binaries and active galaxies. , 359 (1):345–362, May 2005. doi: 10.1111/j.1365-2966.2005.08886.x.

R. Zamanov, G. Latev, S. Boeva, J. L. Sokoloski, K. Stoyanov, R. Bachev, B. Spassov, G. Nikolov, V. Golev, and S. Ibryamov. Optical flickering of the recurrent nova RS Ophiuchi: amplitude-flux relation. , 450(4):3958–3965, July 2015. doi: 10.1093/mnras/stv873.

R. K. Zamanov et al. UBVRI observations of the flickering of RS Ophiuchi at Quiescence. *Mon. Not. Roy. Astron. Soc.*, 404:381, 2010. doi: 10.1111/j.1365-2966.2010.16289.x.

J. Zhou, S. Bi, J. Yu, Y. Li, X. Zhang, T. Li, L. Long, M. Li, T. Sun, and L. Ye. Detection of solar-like oscillations in subgiant and red giant stars using 2 minute cadence tess data. *The Astrophysical Journal Supplement Series*, 271(1):17, feb 2024. doi: 10.3847/1538-4365/ad18db. URL https://dx.doi.org/10.3847/1538-4365/ad18db.
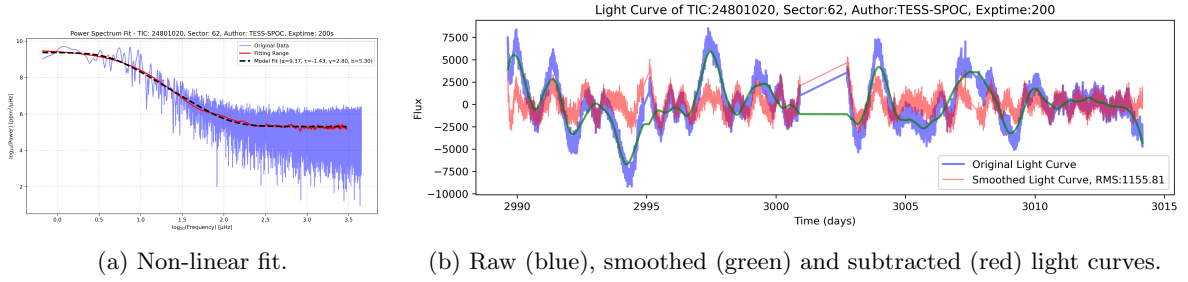
A Light Curves and periodograms

(a) Non-linear fit. (b) Raw (blue), smoothed (green) and subtracted (red) light curves.

Figure 20: Example graphs for a low Binarity Likeness control sample AGB.

(a) Non-linear fit. (b) Raw (blue), smoothed (green) and subtracted (red) light curves.

Figure 21: Example graphs for a high Binarity Likeness control sample AGB. Very high γ and very low τ.

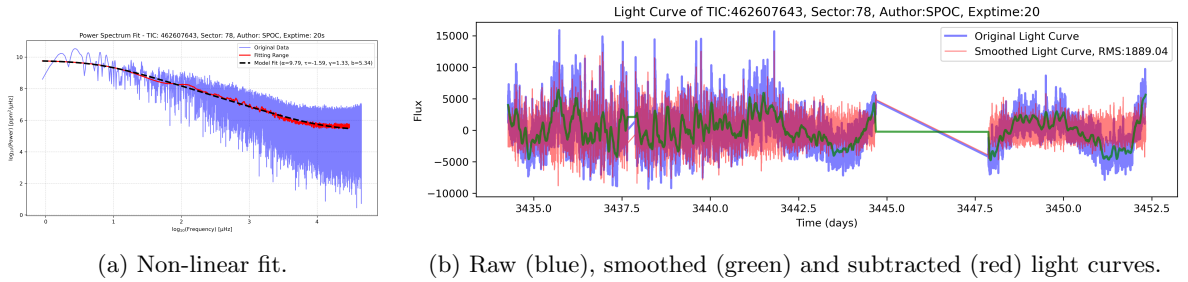(a) Non-linear fit. (b) Raw (blue), smoothed (green) and subtracted (red) light curves.

Figure 22: Example graphs for a flickering source from Merc, J. et al. (2024).